4-17-2017

A Small-Scale Hybrid Wind Turbine and Fuel Cell Electrical Generator

Suman Acharya

A SMALL-SCALE HYBRID WIND TURBINE AND FUEL CELL ELECTRICAL GENERATOR

by

Suman Acharya

A Thesis

Submitted in Partial Fulfillment of the

Requirements for the Degree of

Master of Science

Major: Mechanical Engineering

The University of Memphis

May 2017

DEDICATION

This thesis is dedicated to my mother, my father and my wife for giving me the opportunity to succeed and who have supported me throughout my life, and for those who believed in me.

ACKNOWLEDGEMENT

First and foremost, I offer my sincerest gratitude and respect to my advisor Dr. Jeffrey G. Marchetta, Department of Mechanical Engineering, for accepting me as a master's candidate, for his invaluable guidance, encouragement, and for his insight throughout the course of this research. I consider myself extremely fortunate to have had the opportunity of associating myself with him. I would also like to thank Dr. John I. Hochstein and Dr. William S. Janna for serving on my thesis committee.

I wish to express my deepest gratitude to Barry Wymore and Jason Presley who helped me with the fabrication and assembling required to carry out this project. I am also thankful to Tom Wyatt from the Electrical and Computer Engineering department for his guidance in setting up the electrical circuit. I greatly appreciate and convey my heartfelt thanks to my colleagues, dear ones and all those who helped me in the completion of this work.

I am especially indebted to my parents, beloved wife, and sisters for their love, sacrifice, and support. They have set the great examples for me about how to live, study and work hard. My sincere thanks goes to those who have guided, encouraged, and extended their helping hands towards me in various ways during my tenure at the University of Memphis.

ABSTRACT

The global increase in energy demand combined with socioeconomic, political and environmental concerns associated with fossil fuels have increased the interest in alternative sources of energy. A wind turbine converts mechanical energy in the wind into the kinetic energy and to electrical energy. A fuel cell is an electrochemical device that converts fuel and oxidant into electricity and water with up to 83% efficiency. Flooding is a limitation of fuel cells and occurs when water cannot be expelled from the polymer electrode membrane at a sufficient rate to maintain a continuous reaction. This study presents a small-scale prototype hybrid wind turbine/fuel cell system that combines two demonstrated alternative energy technologies in an effort to achieve a higher efficiency electrical generator through the reduction of flooding in the fuel cell. In the hybrid system, the fuel cell is mounted on the rotating shaft of the wind turbine to increase the rate of water removal in the fuel cell membrane. The small-scale hybrid wind turbine and the fuel cell electrical generator is tested in a wind tunnel and power measurements are obtained for the hybrid system over a range of wind speeds. The experimental results show that the proposed hybrid system is technically feasible and that the rotation increases the fuel cell efficiency up to 10% when compared to a stationary fuel cell.

TABLE OF CONTENTS

LIST OF FIGURES

Figure **Page**

NOMENCLATURE

F_{bc} = hydrophobic force

θ = average static angle

F_c = centrifugal force

R = radius of rotation

ψ = mass flow

E = cell voltage

I = current

F = Faraday's constant

N = number of electron transfer

dH = total energy of system

ds = change in entropy

ΔG^o = Gibbs free energy

Q_{in} = enthalpy of formation

A = swept area of rotor

C_p = power coefficient

P_{wt} = power of wind turbine

P_{fc} = power of fuel cell

H = efficiency

m = mass

ΔP = pressure differential

δQ = heat transfer

U = internal energy

I. INTRODUCTION

A. Motivation

Energy is a fundamental necessity for modern society and industrial growth. As the world's population continues to grow, energy consumption will continue to rise. Subsequently, the need to expand access to energy in new ways is also growing, as resources become limited and environmental concerns increase. Conventional energy sources based on oil, coal, and natural gas have proven to be highly effective drivers of economic progress, but can be detrimental to the environment and to health. The wind turbine is a device that converts kinetic energy available in the wind to the electrical energy. Wind power, as an alternative to burning fossil fuels, is a renewable option, which can be widely distributed and produces no greenhouse gas emissions during operation [1].

Another alternative source of electric power is the fuel cell (FC) [2]. The fuel cell is an electrochemical device that converts fuel and oxidant into electricity directly, with up to 83% theoretical efficiency and low environmental impact [3]. Similar to a combustion process, fuel cells convert chemical bonds into electrical energy. The difference is that while combustion processes transform chemical energy into heat, which is further converted into electricity in a power plant, fuel cells convert chemical bond energy directly into electrical energy. Therefore, the fuel cell process is not restricted by the Carnot efficiency and is potentially more efficient than the internal combustion engine. Fuel cell operation is similar to that of a battery, except that in a fuel cell system, the reactants and products are constantly supplied and removed. Fuel cells are an attractive alternative for applications including but not limited to laptop computers, cell phones, auxiliary and backup power generation for stationary power applications, and automotive vehicles fuel cells.

Fuel cells are commonly classified by the type of electrolyte used in the cells; proton exchange or polymer electrolyte membrane (PEMFC), alkaline (AFC), phosphoric acid (PAFC), molten carbonate (MCFC) and solid oxide (SOFC). The PEMFC seems to be the most attractive option for mobile applications because of its low operating temperature, solid phase electrolyte and ability to operate air with CO_2 [4]. Among the various types of fuel cells, more revolutionary advances have been made for the PEMFC. As such, PEMFCs are the leading candidate to replace aging alkaline fuel technology [5]. PEMFC are constructed using polymer electrolyte membranes (notably Nafion®) as proton conductor and Platinum (Pt) as a catalyst. Their noteworthy features include low operating temperature, high power density, and easy scale-up, making PEMFCs a promising candidate as the next generation power sources for both stationary and portable applications.

Water flooding is a major disadvantage of power degradation in PEMFCs. The proton conductivity is directly proportional to the water content. Various problems arise if the membrane is under hydrated or if the fuel cell is flooded. Flooding occurs when excess water blocks the electrodes or the gas diffusion layer [2], thus preventing the gaseous fuel and oxygen from reaching the catalyst. Therefore, water management, to which many engineers and scientists have recently paid particular attention to, has been a critical challenge for a high-performance fuel cell design and optimization. The wind turbine is introduced herein as a possible alternative to solve the problem of water flooding in fuel cells. This is based on the physics of water extrusion from pores, tubules, and cavities by the use of centrifugal force. If the fuel cell is mounted on the shaft of the wind turbine and rotated, it is believed that rotation will improve the performance of the fuel cell by extracting the water that is flooded. A common

household example is the rotating drum of a washing machine that extracts water from its load during the spin phase.

B. Research Objective

The objective of this research is to design and construct a small-scale prototype hybrid wind turbine and fuel cell electrical generator and test the feasibility and effectiveness of the system to control water flooding in the fuel cell and increase the power generation. The design and construction of the hybrid system will be discussed. The experiment setup and subsequent results from these experiments will be used to assess the feasibility of the hybrid system.

II. LITERATURE REVIEW

The very first fuel cell effect was discovered by Christian Friedrich Schoenbein in 1838 [6]. In 1839, William Robert Grove invented the first fuel cell, which started the development of the clean energy converter that is currently in use today. Researchers have since attempted to develop analytic and empirical models of fuel cells to optimize their design. Analytical efforts that focus on the specific aspects of heat, mass and momentum transport characteristics have been proposed in the past in order to increase the performance of fuel cell [7]. Unfortunately, fuel cells are complex systems and are difficult to completely model analytically. Modern analytical models of the fuel cell have a theoretical basis but still rely on empirical constants. Empirical models, on the other hand, have a limited theoretical basis and are curve-fits to experimentally obtained measurements.

Most modeling efforts have focused on the various parts of the PEM fuel cell which include the gas diffusion layer/gas flow channel (reactant transport), the polymer electrolyte membrane (proton and water transport), and the catalyst layer (reaction site) [8]. Typical PEM fuel cell models consist of transport equations for these respective parts and may include water transport and heat effects. Nguyen and White's earlier model [9] discerned the most important variables in the fuel cell that determines overall performance. They found that the important factors are gas mass flows (pressure and stoichiometry of the inlet gasses), operating temperature of the fuel cell, and the relative humidity.

Water transport problems within the electrolyte membrane are related to osmotic drag, back diffusion, water flux and membrane hydration [10]. Researchers have developed methods to increase the transport of water by controlling the hydrophobicity of GDL surface [11],

introducing magnetic microparticle to the cathode [12] and using absorbent wicks for controlled humidification of gasses [13]. These solutions were found to be inefficient and cost prohibitive.

For the present study, PEM fuel cells are mounted to the rotating shaft of a wind turbine to manage water in the fuel cell using centrifugal force. Centrifugal force is a physical phenomenon caused by inertia in which an object moving in a curve is pushed away from the curve's center [14]. A washing machine drum in which water is extracted from the load by constant rotation can be taken as an example for this physics principle. In this study, the fuel cell is mounted on the main speed shaft of a wind turbine to create the rotation required, the power output of the PEMFC and the wind turbine will be analyzed.

III. BACKGROUND

A. PEM Fuel Cell Structure

Like other fuel cells, the basic element of a PEMFC is the cell. As shown in Figure 1, the cell consists of four major structures including electron collection plates called electrode, gas diffusion layers (GDL), a catalyst coated electrolyte membrane and a closed electrical circuit between the two collection plates. Hydrogen is supplied to the cell through channels in the collection plate on the anode side of the electrolyte membrane. It then diffuses through the GDL to the surface of the electrolyte membrane where the first half of the electrochemical reaction occurs. As the name suggests, one purpose of the GDL is to assist gas diffusion across the entire surface of the catalyst layer on the electrolyte membrane. Without the GDL, the only areas of the membrane surface where reactions could occur would be those areas in direct contact with the reactant gas flow channels, and there would be no conductor present to carry electrons away from the reaction sites.

The electrolyte membrane is made from a polymer material that has charge sites for proton transport. This is generally accomplished by adding a sulphonic acid functional group to existing polymers. For example, the most widely used electrolyte membrane in PEMFCs is known by trade name Nafion®. Nafion® has the same backbone structure as Teflon® but has added sulfonic acid groups. Without significant amounts of water in the membrane, Nafion's® ion conductance significantly diminishes. Much of the water needed to maintain ion conductance comes from the cathode reaction. Many systems utilize reactant gas humidification to maintain membrane hydration.

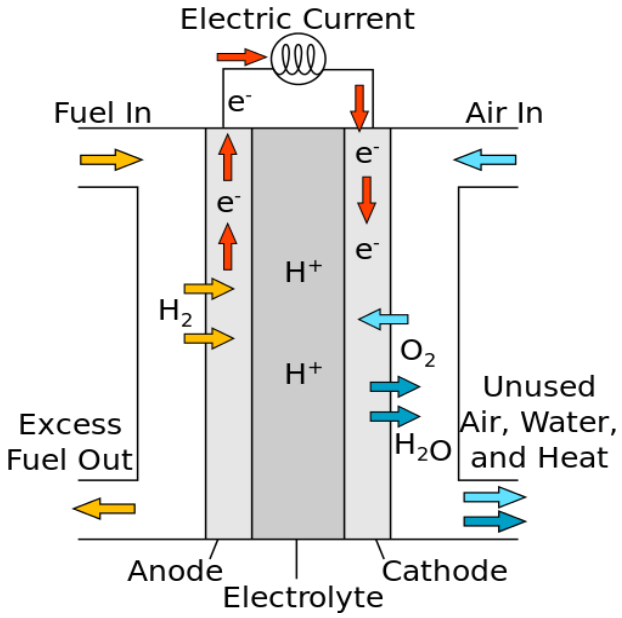

Figure 1. PEM fuel cell structure [15]

Similar to the anode, oxygen or air flow through channels in the collection plate on the cathode side of the electrolyte membrane. The oxygen also flows through a GDL to help increase the active surface area of the electrolyte membrane surface. The cathode is where the second half of the electrochemical reaction occurs and where the product water is created. The product water is removed from the cell through the same channels in the cathode collection plate that supply the cell with oxygen.

B. The Electrochemical Reaction

The electrochemical reaction of the PEMFC occurs in two places at two different locations inside of the cell. The first stage of the reaction occurs at the anode. Hydrogen is brought into the cell through the flow channels where it diffuses through the GDL to the catalyst layer on the electrolyte membrane. The first half of the electrochemical reaction takes place where there is material from the electrolyte membrane (proton conductor), catalyst, GDL (electron conductor), and hydrogen present in one area at a microscopic level. This is the place where the catalyst

breaks the hydrogen molecules into hydrogen ions (protons) and electrons. The chemical reaction can be written as [15]

$$H_2 \rightarrow 2H^+ + 2e^- \quad (1)$$

The hydrogen ions pass through the electrolyte membrane, which is conductive to protons but not electrons. Since the electrons cannot pass through the membrane, they are carried away from the reaction site through the electrically conductive GDL, into the anode collector plate and then through an electric circuit. The hydrogen ions pass through the electrolyte membrane to the cathode. Here the electrons from the electric circuit connected to the anode and oxygen gas meet. A catalyst combines the oxygen, hydrogen ions, and electrons into water molecules, which exit the cell as exhaust through the flow channels in the cathode collector plate. This reaction can be written as:

$$2H^+ + 2e^- + \frac{1}{2}O_2 \rightarrow H_2O \quad (2)$$

Combining equation (1) and (2) gives the overall reaction of the fuel cell and can be written as

$$H_2 + \frac{1}{2}O_2 \rightarrow H_2O \quad (3)$$

From equation (3), it can be seen that water is a product of the reaction.

Farhat developed a novel approach that illustrates the effect of the rotary fuel cell based on the analysis of the forces exerted on a drop of water at the tip of a capillary tube of the fuel cell [7]. Before any rotation is introduced, the superhydrophobic matrix of the cathode is responsible for ejecting any excess of water from the fuel cell. However, once the fuel cell floods, water will remain engulfed in the fuel cell unless each droplet overcomes a hydrophobic force, $F_{bc,}$ which is given by the equation:

$$F_{bc} = 2\pi r\gamma \cos\theta \tag{4}$$

where r is the radius of the capillary, γ is the surface tension of water, and θ is the average static angle measured at the superhydrophobic surface of a commercial fuel cell electrode [7].

Figure 2 shows different types of forces analyzed by Farhat. In the presence of any hydrophilic tubule, all water with a hydrophilic capillary force of the same magnitude and with complementary angles would be captured [7]. The weight of water is the other force applied (F_w) on the droplet which can be shown as;

$$F_w = mg \tag{5}$$

where m is the mass of the droplet and g is the force of gravity. A new force called centrifugal force (F_c) is introduced on the Z-axis once rotation has been induced which is given by Equation 6.

$$F_c = m\omega^2 R \tag{6}$$

where ω is the angular velocity, and R is the radius of rotation.

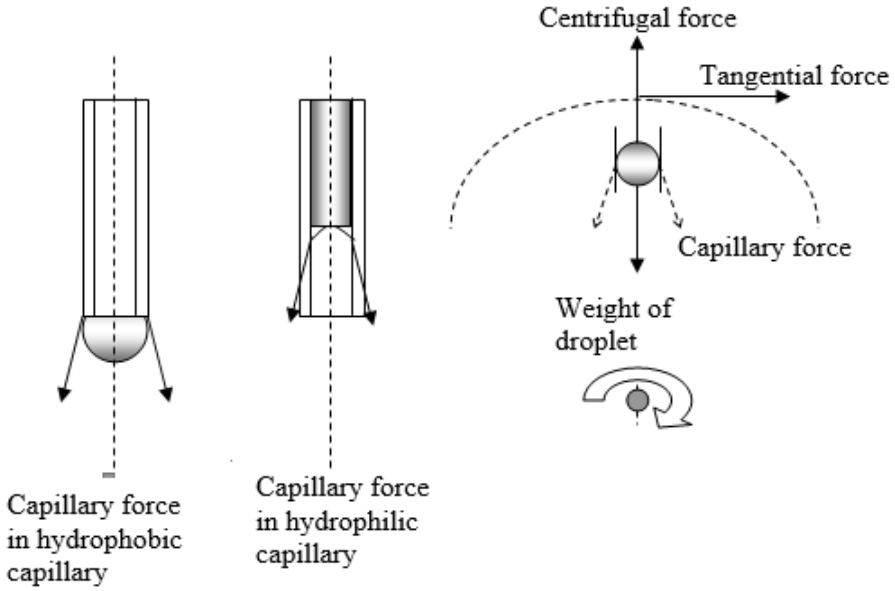

Figure 2. Farhat experiment showing forces [7]

To analyze the mass flow,ψ across capillaries, the forces acting on the z-axis, F_{bc} and, F_w are considered. The forces have the same direction counterbalancing the centrifugal force, F_c. The Poiseuille's formula given below determines the mass flow,ψ. The mass flow is a function of the pressure differential across a group of capillaries N with area A, ρ is the density of water 1000 kgm^{-3}, η is the viscosity of water which is equal to 1.3 x 10^{-3}, kgm^{-1} s^{-1}, L is the length of capillary in m, r is the radius of the capillary, and ΔP is the pressure drop across the capillary: [7] [14]

$$\Psi = \frac{NA\rho r^4}{8\eta L}\Delta P \tag{7}$$

The pressure drop ΔP is expressed as:

$$\Delta P = \frac{\Delta F}{A} = \frac{\left(m\omega^2 R - (2\pi\gamma\cos\theta + mg)\right)}{A} \tag{8}$$

Now, substituting equation (8) in equation (7) gives equation (9)

$$\Psi = \frac{N\rho r^4}{8\eta L}\left(m\omega^2 R - (2\pi\gamma\cos\theta + mg)\right) \tag{9}$$

Using Equation 9 Farhat found that to extract any excess water from the fuel cell, a critical rotation must be reached [7]. Farhat setup an experiment, as shown in Figure 3, to validate his analytic model. He used a commercial fuel cell of a maximum output power 27 $mWcm^{-2}$ under ambient conditions mounted on a propeller and driven by an electric motor. The fuel cell was fixed 4 inches from the center of rotation and was supplied with hydrogen gas from a small bottle during rotation. Oxygen was supplied from atmospheric air at the cathode. Farhat determined the critical rotation for his experiment was 375 rpm. Therefore, at any rotation greater than this critical rate, the centrifugal force generated, should remove the excess water from the fuel cell.

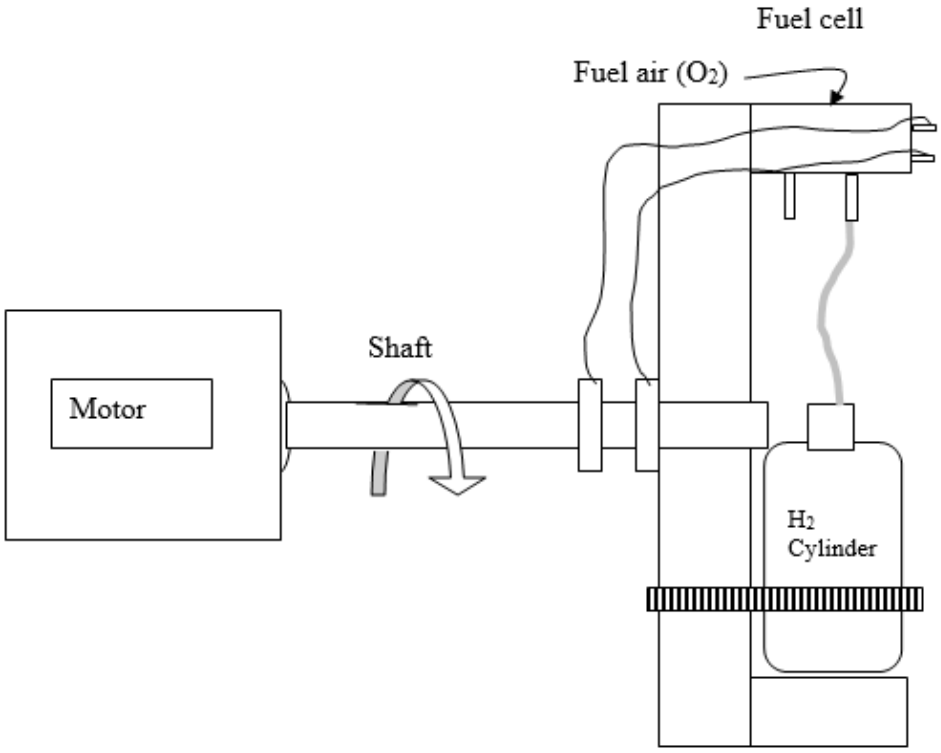

Figure 3. Schematic diagram of Farhat experiment

The efficiency of a fuel cell is determined by the ratio of the actual voltage at some current density to the maximum voltage attained under no load (open circuit) conditions [4]. The basic energy conversion process occurring in a fuel cell, shown in Figure 4, can be described by the following equation.

$$Chemical\ energy\ of\ fuel\ cell = Electrical\ energy + Heat\ energy \qquad (10)$$

The energy that is produced during the reaction at the electrodes is known as input energy. The energy balance of Equation 10 is done using first and second law of thermodynamics. By using the first law of thermodynamics for a control volume, the change can be approximated by the change in enthalpy.

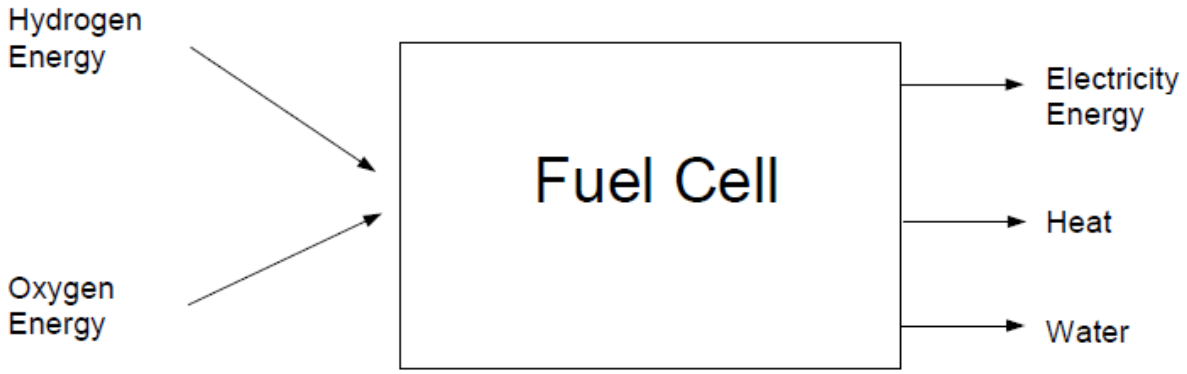

Figure 4. Fuel Cell input and output

In the electrochemical reaction of a fuel cell, work is obtained from the transport of electrons across the potential difference, not by mechanical means [4][16].

$$\Delta E = Q - W \tag{11}$$

where $\Delta E = \Delta KE + \Delta PE + \Delta U + \Delta(PV) = \Delta H$

The electrical work can be expressed as:

$$W = EI\Delta t \tag{12}$$

where E is the cell voltage and I is the current. In the fuel cell reaction, the electrons travel from the anode to the cathode, thus generating a current. The amount of electricity ($I\Delta t$) transferred during the reaction is determined by the product of the number of electrons transferred (N) and Faraday's constant (F). Therefore, the electrical work can be calculated as:

$$W = NFE \tag{13}$$

Substituting into the first law in equation (11), yields:

$$\Delta E = \Delta H = Q - NFE \tag{14}$$

The heat transfer component in Equation 14 is evaluated using the second law of thermodynamics. Assuming the fuel cell is reversible and thus behaves as an ideal electrochemical apparatus, the heat transferred can be expressed as:

$$Q = T\Delta S \tag{15}$$

Thus the combination of the first law and second law analysis gives

$$\Delta H = T\Delta S - NFE \tag{16}$$

For a cell operating reversibly

$$dH = TdS - FEdN \tag{17}$$

Under these conditions, the losses are minimized and the maximum useful work, represented by the Gibbs free energy [4][16], done by a fuel cell is:

$$dG = dH - TdS \tag{18}$$

where *dH* is the total energy of the system and *TdS* is the measure of energy not available for useful work in the system. Consequently, *G* represents the amount of free energy that available to do useful work.

Furthermore, the Gibbs free energy can be related to the chemical energy dissipated during the fuel cell reaction. The electrons released to generate the electrical work are, related to the chemical reaction taking place. So ΔG can also be associated with chemical energy released during the fuel cell reaction. The level of available energy is dependent on temperature and pressure. Typically, a "free energy of formation", ΔG_f or ΔG^o is computed for these reactions, where the free energy is referenced with respect to standard temperature and pressure (STP) conditions. For any reaction, the Gibbs free energy can be calculated as:

$$\Delta G^o = G^o{}_{products} - G^o{}_{reactants} \tag{19}$$

The Gibbs Free Energy equation for the hydrogen, oxygen reaction in fuel cells is shown by equation [5] [4]

$$\Delta G^o = (\Delta G^o)_{H_2O} - (\Delta G^o)_{H_2} - \frac{1}{2}(\Delta G^o)_{O_2} \tag{20}$$

The reversible open circuit voltage can be calculated based on ΔG^oas:

$$E = \frac{\Delta G^o}{NF} \tag{21}$$

It is well known that fuel cell efficiency is not limited by Carnot efficiency of the cycle [2]. Since fuel cells use materials that reacted to release energy, the efficiency of a fuel cell can be described as the ratio of the electrical energy produced by the heat that is produced by burning fuel (its enthalpy of formation or Δh_f) [4].

From the basic definition of efficiency, it can be shown that:

$$\eta = \frac{W}{Q_{in}} \tag{22}$$

where W is given by ΔG (orNFE) and Q_{in} is the enthalpy of formation of reaction taking place. Since two values can be often computed depending on the state of reactant, the larger of the two values i.e. higher heating value (HHV) is used.

$$\eta = \frac{\Delta G}{HHV} = \frac{NFE}{HHV} \tag{23}$$

The maximum efficiency occurs under open circuit conditions (reversible) when the highest cell voltage is obtained.

$$\eta_{max} = \frac{\Delta G^o}{HHV} = \frac{NFE^o}{HHV} \tag{24}$$

The maximum efficiency of a fuel cell under the ideal condition as determined by Eq. 24 is 83% [4]. In this research, the manufacturer of the fuel cell used in the experiments has set the maximum rated output power from a fuel cell as 150 mW. Thus, the rated maximum power output under the ideal condition is:

$$P_{FC,ideal} = 150 \times 2 = 300\ mW \tag{25}$$

However, power output from the fuel cell ($P_{FC,actual}$) can be calculated using experimental measurements of the voltage and current output:

$$P_{FC,actual} = V \times I \tag{26}$$

where *V* is voltage measured and *I* is the current measured at a corresponding voltage level. Thus, the actual efficiency of the fuel cell can be calculated as:

$$\eta_{FC,actual} = \frac{P_{FC,actual}}{P_{FC,ideal}} \tag{27}$$

C. Wind Power

Wind energy is recognized worldwide as cost-effective, environmentally friendly renewable source of energy. The United States has an abundance of the potential sites where electricity can be generated using wind power [17]. Wind power is growing rapidly in America. The wind has accounted for 33% of all newly installed electricity generation capacity in the years spanning from 2006 to 2013 as per Wind Vision Report [18]. The report states that the United States now gets about 4.6 percent of its electricity from wind power. The price of wind energy is projected to be directly competitive with conventional energy technologies within the next decade. Wind energy could be a viable source of renewable electricity in all 50 states and could support more than 600,000 jobs in manufacturing, installation, maintenance and supporting services by 2050. The report also shows that wind energy could save $508 billion from reduced pollutants, $280

billion in natural gas costs and 260 billion gallons of water that would have been used by the electric power sector by 2050. Currently, the wind is the third biggest source of generation in the Southwest Power Pool (SPP) region [19], making up about 15 percent of capacity in 2016 behind natural gas and coal. This is the first time that wind was even briefly more than 50 percent of the source of electric power at any US grid, according to SPP. Figure 5 shows the projected growth of the wind industry over the next 35 years in the continental United States.

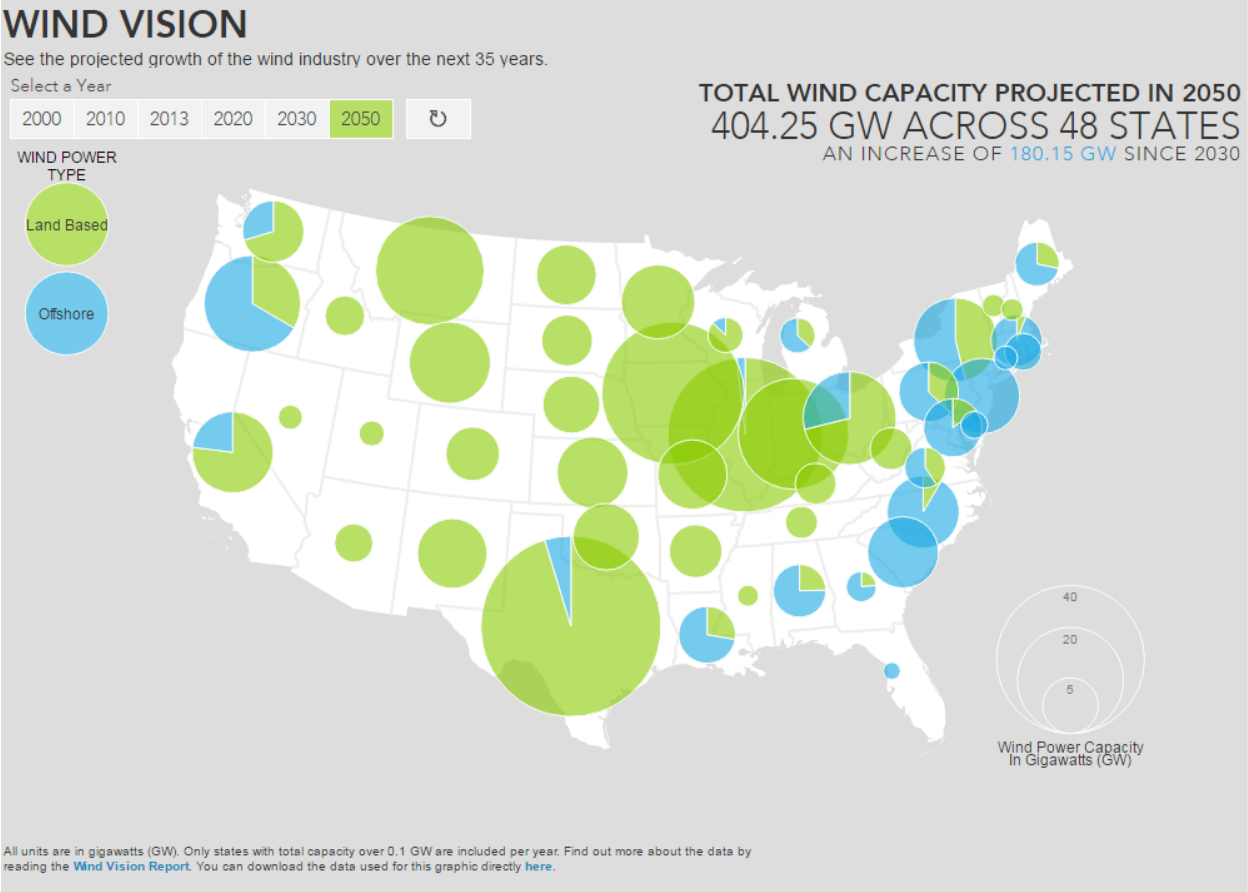

Figure 5. Projected growth of the wind industry over the next 35 years in the US [18]

Figure 6 shows major components of a wind turbine. The main components are the tower, the nacelle, and the rotor [20]. Most current commercial turbine rotors consist of two or three fiberglass blades that are attached to the hub. The rotor is usually connected to a low-speed shaft within the nacelle that then drives the high-speed shaft by a system of gears. The nacelle houses

most of the mechanical components such as the drivetrain, gearbox, transformer, and generator. The nacelle is located at the top of the tower of the wind turbine. The nacelle is equipped with a series of mechanisms that allow it to adjust its position to face the wind. Towers are made up of steel and have tubular or lattice structures. The height of the tower is a fundamental component of a turbine as higher wind speeds occur at higher altitudes.

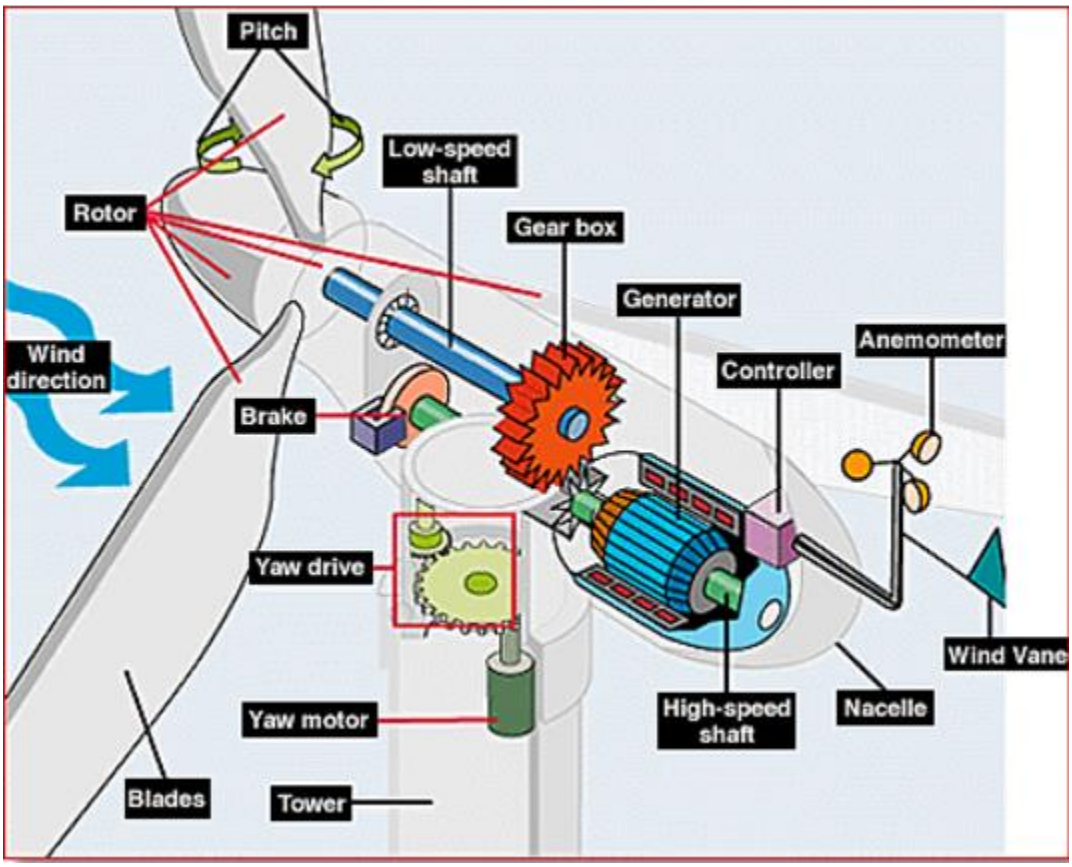

Figure 6. Wind turbine components [21]

Wind turbines convert kinetic energy into electrical energy. First, the kinetic energy is converted into mechanical energy and that mechanical energy into electrical energy [22]. The energy available in the wind turbine mainly depends on the wind speed and the swept area of the rotor of the turbine. The kinetic energy, E, of any object having mass, m, and velocity, v, is equal

to the work done, *W*, in displacing that object from rest to a distance, s under a force, *F*, is given as [23]:

$$E = w = Fs \tag{28}$$

However, according to Newton's second law of motion, the expression for force is

$$F = ma \tag{29}$$

Substitution of equation (29) into equation (28) yields the following equation:

$$E = mas \tag{30}$$

The equation of motion is as follows which give the acceleration of an object as:

$$v^2 = u^2 + 2as \tag{31}$$

Solving for acceleration gives:

$$a = \frac{v^2 - u^2}{2s} \tag{32}$$

Since the initial velocity of an object is zero, $u = 0$, equation (32) reduces to

$$a = \frac{v^2}{2s} \tag{33}$$

Substituting equation (33) into equation (30) yields the kinetic energy of a mass in motions as:

$$E = \frac{1}{2}mv^2 \tag{34}$$

The power, *P*, in the wind is given by the rate of change of energy with respect to time, *t*, as:

$$P = \frac{dE}{dt} = \frac{1}{2}v^2\frac{dm}{dt} \tag{35}$$

The mass flow rate is given by:

$$\frac{dm}{dt} = \rho A \frac{dx}{dt} \tag{36}$$

where ρ is the density of air, A is the swept area of the rotor of wind turbine and $\frac{dx}{dt}$ is the rate of change of distance with time, which is also called velocity, *v* as:

$$\frac{dx}{dt} = v \tag{37}$$

Hence the mass flow rate is found as:

$$\frac{dm}{dt} = \rho A v \tag{38}$$

Thus, the power from equation (35) is defined as:

$$P_{wt,ideal} = \frac{1}{2}\rho A v^3 \tag{39}$$

A German physicist Albert Betz concluded in 1919 that no wind turbine can convert more than 16/27 (59.3%) of the kinetic energy of the wind into mechanical energy turning a rotor [24]. To this day, this is known as the Betz Limit or Betz' Law. The theoretical maximum power efficiency of any design of wind turbine is 0.59 (i.e. no more than 59% of the energy carried by the wind can be extracted by a wind turbine). This is called the "power coefficient" and is defined as $C_{p_{max}} = 0.59$.

In addition, wind turbines cannot operate at this maximum limit. The $C_p$value is unique to each turbine type and is a function of wind speed. Once various engineering requirements of a wind turbine are incorporated like strength and durability, the real-world limit is well below the Betz Limit with typical values ranging from 0.35-0.45 in the best-designed wind turbines. By the time taken other components with losses, e.g. the gearbox, bearing, and generator, are considered in a complete wind turbine system only 10-30% of the power of the wind is ever actually

converted into usable electricity. Hence, the power coefficient needs to be factored in Equation (39) and the extractable power from the wind is given by:

$$P_{wt,ideal} = \frac{1}{2}\rho A v^3 C_p \tag{40}$$

Wind currents originate from the radiation emitted by the sun. The changes in elevation and geography in earth generate an uneven rate of heat absorption; therefore, creating different wind speeds in different conditions. According to these conditions, wind speeds fluctuate throughout the day and all year long as a function of the exposure to the sun's radiation. Areas with annual average wind speeds around 6.5 m/s and greater at 80-m height are generally considered to have suitable wind resources for wind energy development [14]. Power can be determined for a wind turbine experimentally by measuring the RPM of the shaft and Torque produced to compute power, P_{wt}.

$$P_{wt,actual} = RPM\ of\ shaft\ \times Torque\ produced \tag{41}$$

Thus for the ideal wind turbine-fuel cell hybrid system, the total power output will be the sum of power output from wind turbine and fuel cell system.

$$Total\ power\ (P) = Fuel\ cell\ Power\ \left(P_{fc}\right) + Wind\ Turbine\ Power\ (P_{wt}) \tag{42}$$

Similarly, the efficiency of the hybrid system is calculated as:

$$\eta_{system} = \frac{P_{wt,actual}+P_{FC,actual}}{P_{wt,ideal}+P_{FC,ideal}} = \frac{(\tau_w \times \omega)+(V \times I)}{\frac{1}{2}\pi r^2 \rho v^3 \times C_p + \frac{\Delta H}{t}} \tag{43}$$

Figure 7 illustrates how the power output from a wind turbine varies with wind speed. At low air speeds, the wind turbine blade does not rotate because insufficient torque is produced. As the air speed increases, the wind turbine rotor begins to rotate and electrical power is generated. The speed at which the turbine first starts to rotate and generate power is called cut in speed of the

wind turbine. Generally, the cut in speed is between 3 to 4 meters per second for commercial wind turbines. As the air speed rises above the cut-in speed, the wind turbine rotates at higher RPM eventually producing higher power. However, the power output reaches the design limit of the electrical generator, which is typically between 12 and 17 meters per second and this speed is called rated power output. When the air speed increases above the rated output speed, the force on the turbine continues to rise which increases the risk of damage to the wind turbine rotor. As a result, a braking system is employed to stop the rotor, which is called cut-out speed. The cut-out speed is typically 25 meters per second.

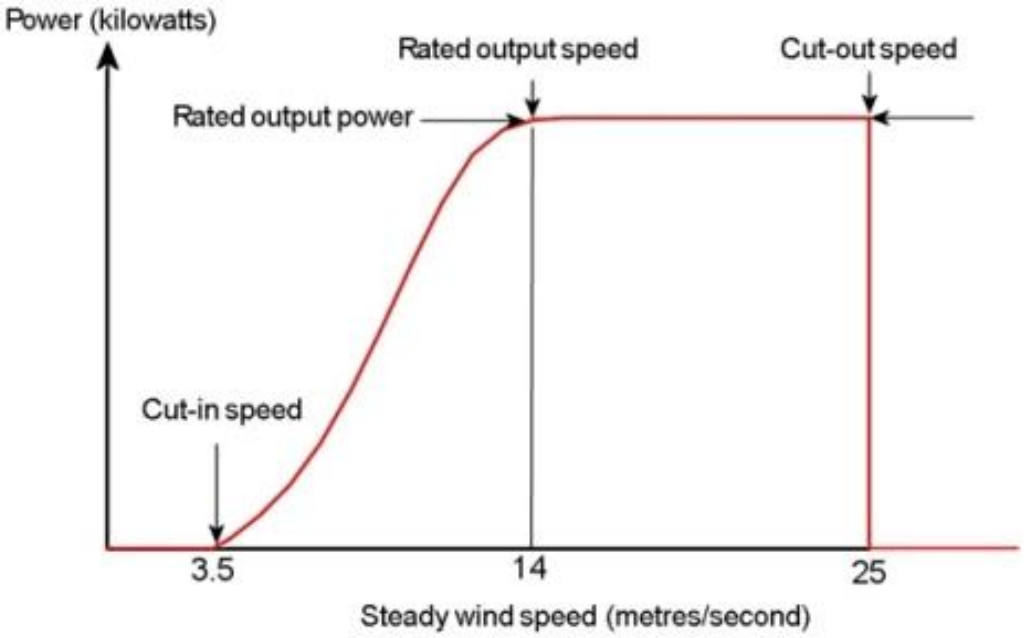

Figure 7. Typical wind turbine power output with steady wind speed [25]

III. EXPERIMENTAL PROCEDURE

The hybrid system prototype was designed in NX CAD, as shown in Figure 8, to best utilize the 144-in^2 area of wind tunnel that is available in the lab. Figure 9 demonstrates that the shaft is made up of 316L stainless steel, is 0.75 inches in diameter, and is connected to the wind turbine blade. There are three rotor blades, which are 4.5 inches in length and have a chord length of 0.75 inches. The blades are mounted on a rotor with round holes located every 120^o apart and have a diameter of ½ inches. The shaft holds a flywheel, stepped hub, two support disks for the hydrogen tanks and magnetic particle brake at the end. Ultra-friction ball bearings are employed with the shaft in order to reduce friction. The system used two commercial F103 fuel cells. The maximum rated power output from one fuel cell is 150mW using air and hydrogen. The fuel cells are mounted on a flywheel, which is mounted on a main shaft of the wind turbine. The flywheel assembly is made of phenolic to shield the shaft and other components from the current generated by the fuel cell. The flywheel is 5 inches in diameter and has two concentric hubs to which aluminum sleeves are fitted with a purpose of conducting the electricity produced by the fuel cell to the graphite brush. Two hydrogen canisters supply hydrogen as fuel to the fuel cell. These hydrogen canisters are mounted parallel to the shaft and held in place with two aluminum disks. The terminal from the fuel cell is connected to an aluminum sleeve fitted into the hub of the flywheel. The silver graphite brush from Helwig Carbon Product Inc. contacts the sleeve. The brushes are housed in a brush holder from Helwig Carbon products Inc. The holders are mounted on a phenolic bracket, which is bolted to the base of the assembly.

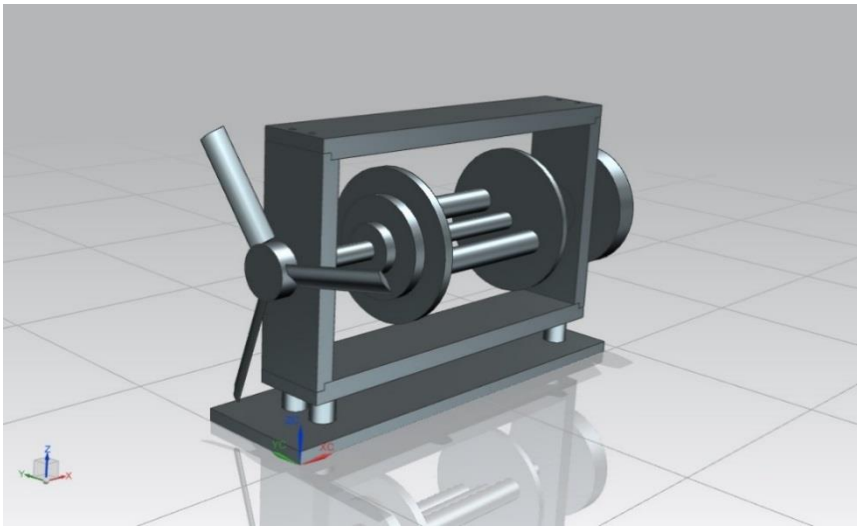

Figure 8. Preliminary design of hybrid system in CAD

The angular velocity of the shaft is measured by using stroboscopic lamp flashes which can vary in frequency up to 6000 flashes per second. When the frequency of the flashes matches the rotational speed, the rotating shaft appears motionless and the shaft rpm is recorded. Wind speed will be measured using a hot wire anemometer which incorporates a very fine wire electrically heated to some temperature above the ambient. Air flowing past the wire cools the wire. A relationship can be obtained between the resistance of the wire and the flow speed because for most metals, the electrical resistance is dependent upon the temperature of the metal. Resistance will be provided as a load to the fuel cell and at that time, the current and voltage across the fuel cell will be measured using a multimeter. A magnetic particle brake is mounted at the end of the shaft to measure the torque output from the wind turbine at different wind speeds. The magnetic particle brake [26] resists the motion of the shaft by applying an electromagnetic field to magnetic particles located inside the brake. The magnetic field binds the particles together to form a magnetic particle slush. The binding of the particles due to magnetic field becomes stronger if the electric current is increased and the brake rotor moves through these

bound particles. When the particles start to bind together, a resistant force will be created on the rotor of the particle brake, which slows, and then eventually stops the output shaft.

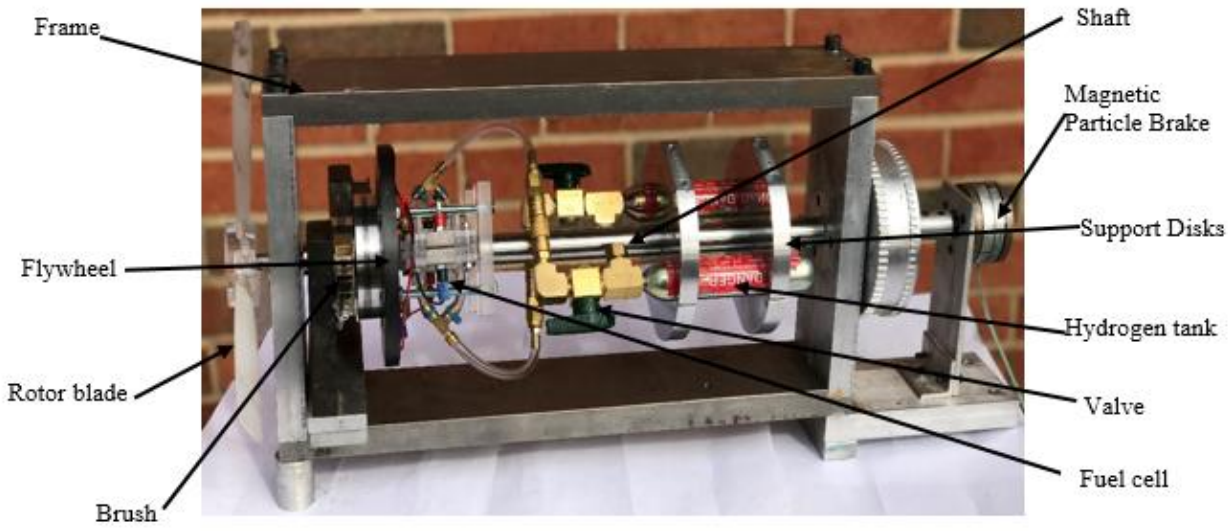

Figure 9. Hybrid System

V. EXPERIMENTAL RESULTS

Torque, RPM, voltage and current measurements obtained from the hybrid wind turbine/fuel cell system were recorded over a range of wind tunnel airspeeds as shown in Figure 10. Seven independent trials of the setup were performed to establish repeatability. Torque and RPM measurements are used to determine the power output of the wind turbine [Equation 41] and current and voltage measurements are used to determine power output from the fuel cells as per [Equation 26]. The fuel cells are considered stationary when the air speed in the wind tunnel is zero or when the shaft is not rotating.

Figure 10. Hybrid system inside wind tunnel

The air speed of the wind tunnel was incrementally increased from 0 mph to 39 mph. The start-up airspeed, which is the wind speed at which the rotor starts turning, was determined to be on average 23 mph in for the hybrid system. At each air speed, the mechanical resistance on the wind turbine shaft was incrementally increased using the magnetic particle brake and RPM of the shaft was measured simultaneously to assess the dynamic torque. Figure 11 shows an example of the torque and RPM measurements, mean and standard deviation, for seven trials at a wind speed of 39 mph. As shown in Figure 11 and Appendix A, the RPM varies linearly with the applied dynamic torque as expected. The power output from the turbine was computed using the

dynamic torque and RPM measurements as exemplified in Figure 12 for an air speed of 39-mph. As shown in Figure 12 and Appendix B is a consequence of the relationship between variables in Equation 41, the power output varies non-linearly with the measured RPM. In Figure 12, for an airspeed of 39 mph, it can be observed that the turbine maximum power output of 3200 mW occurs at 700 RPM. Figure 13 and Appendix C shows the total power output, in mW, of the fuel cells that was computed using voltage and current measurements over a range of RPM measurements of the turbine shaft. At zero RPM, the fuel cells were stationary. As seen in Figure 13, the measured power output of the fuel cells from the stationary position up to approximately 350 RPM remains almost constant. Above 350 RPM, the power increases nonlinearly from approximately 180 mW and peaks at approximately 210 mW representing an overall increase of approximately 10%. The increase in power output above approximately 350 RPM is consistent with the critical rotation observed by Farhat for rotating fuel cell positioning less than 1 cm away from the center of rotation.

The total maximum power output of the hybrid system can be determined for each airspeed by adding the maximum power output of the wind turbine and power output from the fuel cells at the same RPM [Equation 42]. Figure 14 shows the maximum power out of the hybrid system for a range of wind tunnel airspeeds and the maximum power if the fuels cells were not rotating with the wind turbine shaft. It is difficult to discern the increase in total hybrid system power achieved by rotating the fuel cells in this figure because the power output from the turbine is an order of magnitude larger than the power output of the fuel cell. Table 1 shows the mean of the data obtained for seven independent trials and indicates an average 1.7% increase in the total hybrid system power output was achieved by rotating the fuel cells. Overall, the data presented in Table 2 shows the hybrid system efficiency, as computed using Equation 43, is increased by

approximately up to 0.115% when the fuel cells are rotated. It should be noted, however, that the efficiency of the wind turbine is only 1~ 3% on average as shown in Table 2. Table 3 shows the average power output using the experiment measurements for the rotating fuel cells over a range of airspeeds. Calculation of the fuel cell efficiency over a range of airspeeds indicates an average increase of 10% is achieved above the critical rate of rotation when compared to the fuel cell efficiency for the stationary fuel cells.

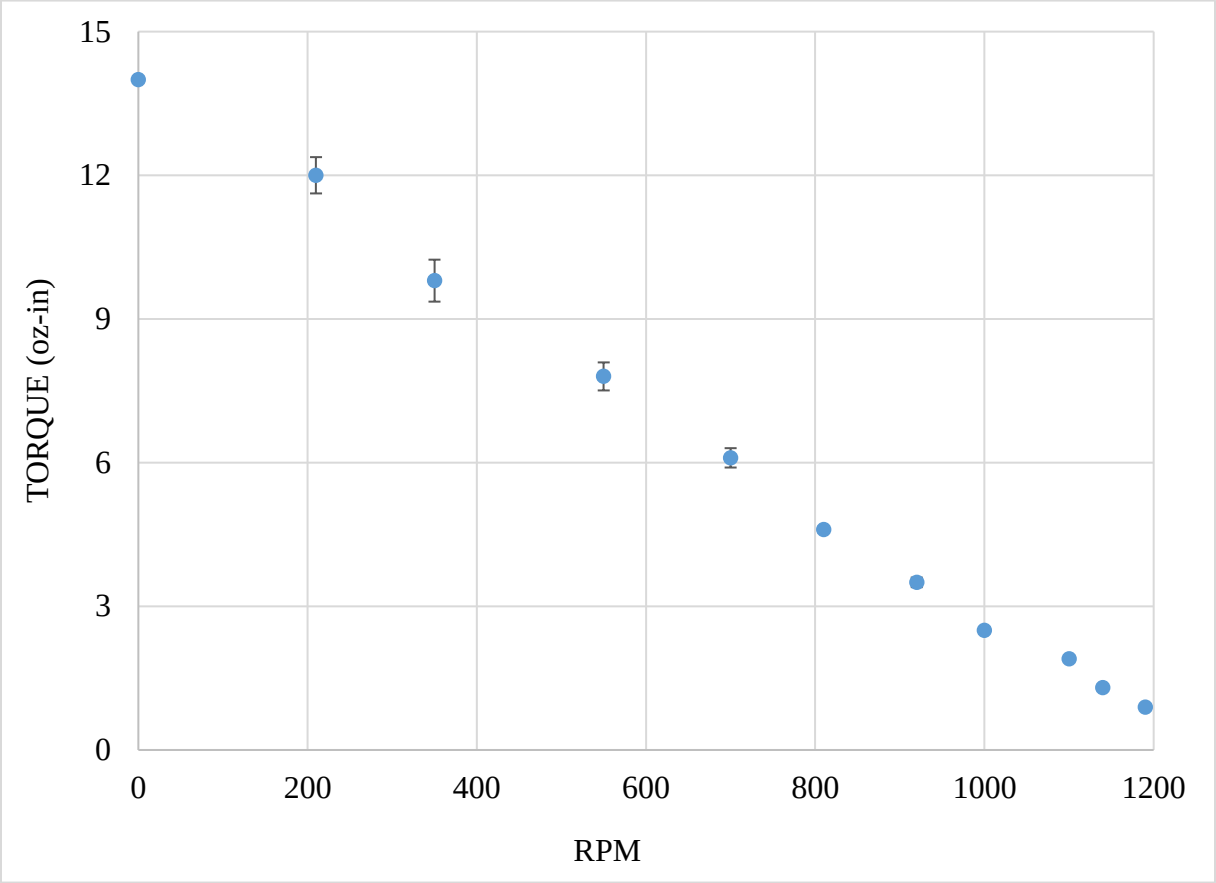

Figure 11. Mean and experiment error of wind turbine shaft torque for varying shaft RPM at 39 mph

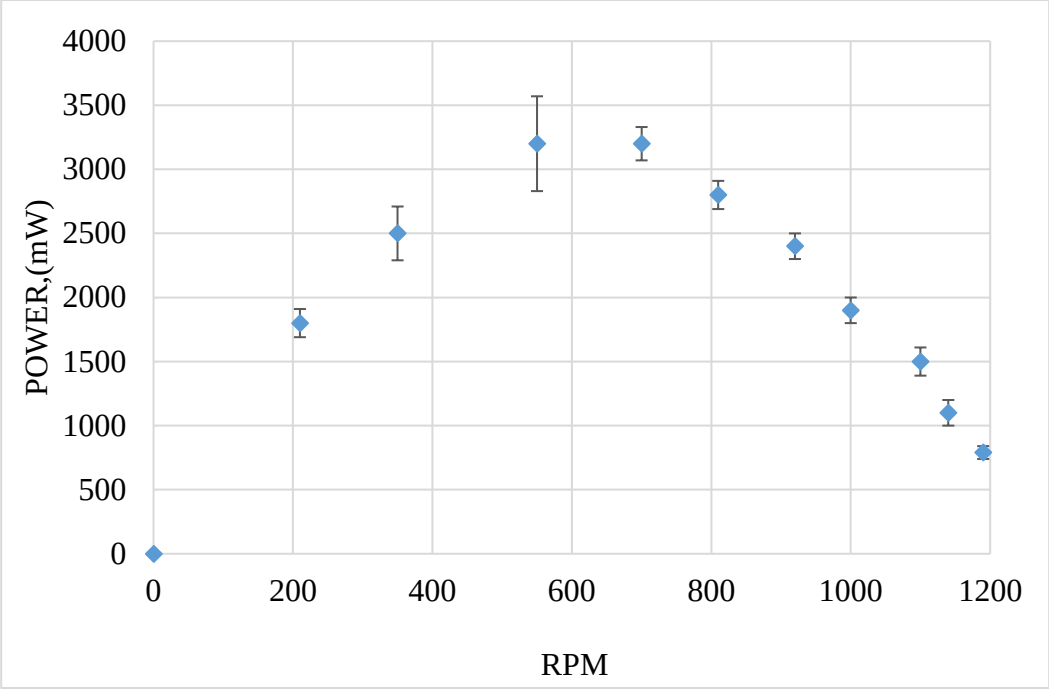

Figure 12. Mean and experiment error of wind turbine power output for varying shaft RPM at 39 mph

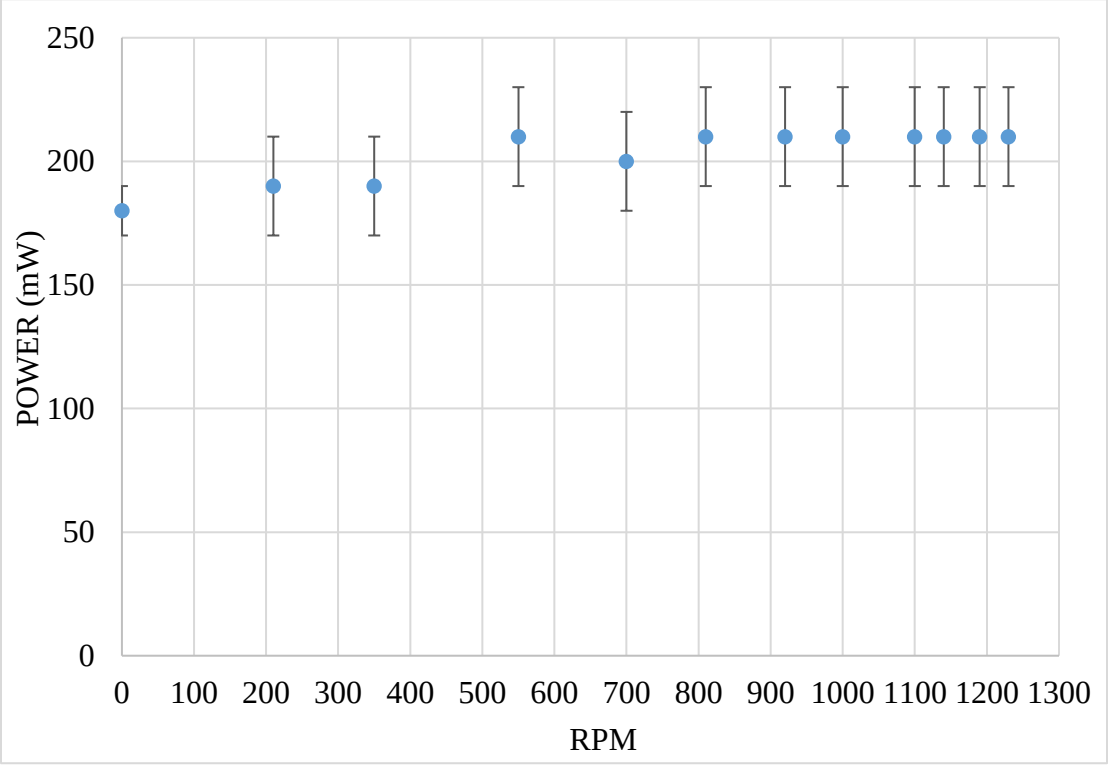

Figure 13. Mean and experiment error of fuel cell power output for varying RPM of the wind turbine shaft at 39 mph

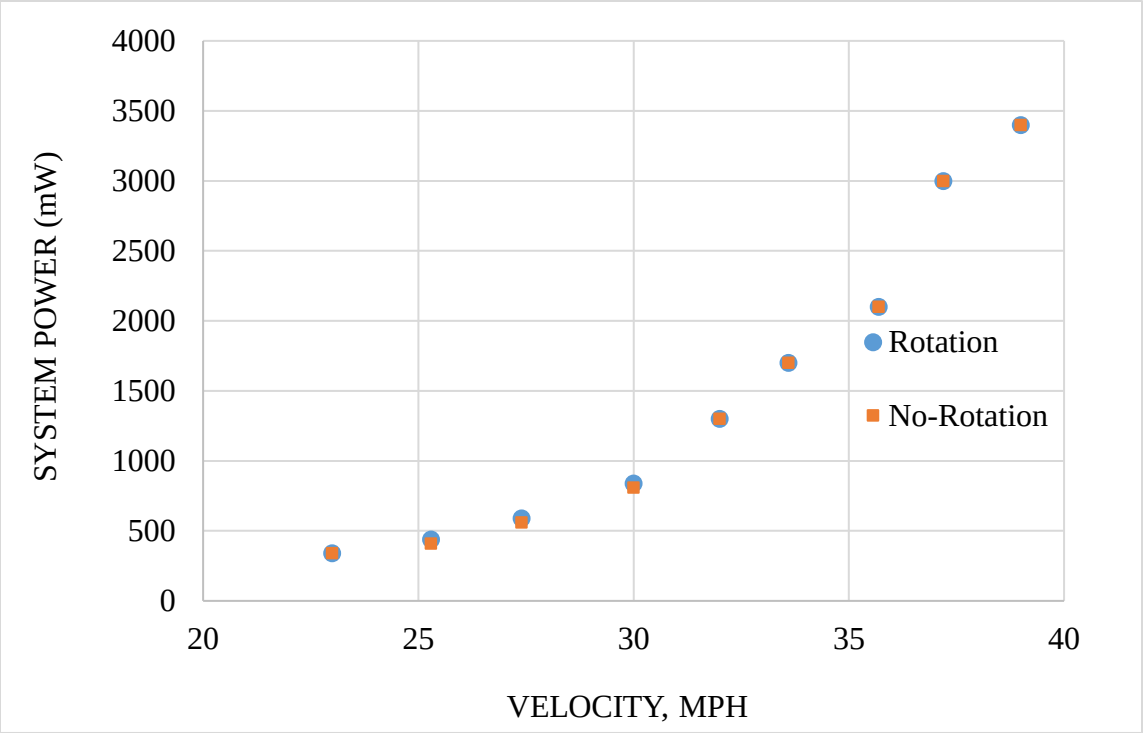

Figure 14. Total hybrid system power output vs wind tunnel air speed for rotating and stationary fuel cells at 39 mph

Table 1. Comparison of power output of hybrid system with stationary and rotating fuels cells

SN	Wind tunnel air speed (mph)	Ideal Hybrid System power (mW)	Actual Hybrid System power (Rotating Fuel Cell)	Actual Hybrid System power (Stationary Fuel Cell) (mW)	Increase in power by rotation
1	39	96000	3400 ± 200	3400 ± 100	0.0%
2	37	83000	3000 ± 200	3000 ± 200	0.0%
3	36	74000	2100 ± 300	2100 ± 300	0.0%
4	34	62000	1700 ± 100	1700 ± 100	0.0%
5	32	53000	1300 ± 100	1300 ± 100	0.0%
6	30	44000	840 ± 90	810 ± 80	3.6%
7	27	34000	590 ± 80	560 ± 70	5.1%
8	25	26000	440 ± 70	410 ± 60	6.8%
9	23	20000	340 ± 80	340 ± 70	0.0%

Table 2. Comparison of efficiency of hybrid system with stationary and rotating fuel cells

SN	Wind Tunnel Air Speed (mph)	Wind Turbine Efficiency (η_{wt})	Fuel Cell Efficiency (Rotating Fuel Cells) (η_{fc})	Fuel Cell Efficiency (Stationary Fuel Cells) (η_{fc})	Increase in Efficiency of hybrid System
1	39	3.3%	70.0%	60.0%	0.000%
2	37	3.4%	70.0%	60.0%	0.000%
3	36	2.4%	70.0%	60.0%	0.000%
4	34	2.0%	70.0%	60.0%	0.000%
5	32	2.0%	70.0%	60.0%	0.000%
6	30	1.4%	70.0%	60.0%	0.068%
7	27	1.1%	70.0%	60.0%	0.088%
8	25	0.9%	66.7%	60.0%	0.115%
9	23	0.8%	60.0%	60.0%	0.000%

Table 3. Comparison of power and efficiency for stationary and rotating fuel cells

SN	Wind Tunnel Air Speed (mph)	Maximum Power Output of Rotating Fuel Cells (mW)	Maximum Power Output of Stationary Fuel Cells (mW)	Increase in Fuel Cell Efficiency
1	39	210 ± 20	180 ± 10	10.0%
2	37	210 ± 20	180 ± 10	10.0%
3	36	210 ± 20	180 ± 10	10.0%
4	34	210 ± 20	180 ± 10	10.0%
5	32	210 ± 20	180 ± 10	10.0%
6	30	210 ± 20	180 ± 10	10.0%
7	27	210 ± 20	180 ± 10	10.0%
8	25	200 ± 20	180 ± 10	6.7%
9	23	180 ± 10	180 ± 10	0.0%

VI. CONCLUSION

A hybrid small-scale wind/fuel cell electrical generator has been designed and tested in a wind tunnel to assess the feasibility of using fuel cells on a rotating shaft to increase total power output. Results presented herein suggest that the use of a wind turbine to provide rotation to a fuel cell can be an alternative for the increasing efficiency of the fuel cell, and subsequently, the efficiency of the wind turbine/fuel cell system. An average increase in the fuel cell efficiency of 10% was observed in this study when the fuel cells were rotated beyond the critical rate of rotation.

An increase in power output at the inception of rotation can be a notable step in the betterment of fuel cell technology, which mitigates fuel cell flooding and addresses water management issues in PEM fuel cells. It cannot be definitively concluded without micro-scale observations of the water flow in the polymer electrode membrane that the rotation directly impacted the water management in the fuel cell in this study; however, the data presented herein and previous work done in this area suggest the correlation is highly probable. For a full-scale design, the combined output can potentially be used to both produce hydrogen fuel for the fuel cell and produce electricity for the grid. The results presented show considerable promise for the hybrid system feasibility. Thus, the use of centrifugal force for the removal of excess water from the fuel cell membrane seems technically feasible.

Commercially available large-scale wind turbines can operate in winds speeds up to 130 mph and typically operate efficiently at wind speeds of 13-17 mph, with start-up speeds between 8-12 mph. The start-up speed of the hybrid system designed for this study was markedly higher at 23 mph than a large-scale commercial turbine; however, the hybrid system has the single shaft. A gearbox is typically used in a commercial wind turbine to increase rotational speed from a low-

speed rotor to a higher speed electrical generator. A common ratio is about 90:1, with a rate 16.7 rpm input from the rotor to 1,500 rpm output for the generator. Some multi-megawatt wind turbines have dispensed with a gearbox. In these so-called direct-drive machines, the generator rotor turns at the same speed as the turbine rotor. This requires a large and expensive generator. For safety reasons, the maximum air speed tested for this study was 39 mph. Considerable effort remains in determining the upward scalability of the design, although some changes, in the small-scale design, such as better balancing the center of inertia on the flywheels, the inclusion of the gearbox, and extension of the turbine rotor hub away from the frame, can likely reduce the start-up air speed. In addition, the wind turbine efficiency for the current design is considerably lower than anticipated. Many changes will be required to increase the wind turbine efficiency so that it is more comparable to a commercial design, which can achieve peak efficiencies around 50%.

If the force of rotation on the fuel cells is directly influencing the water flow in the polymer electrode membrane as hypothesized, the critical rotational speed will be different depending on how far the fuel cells are positioned away from the center of rotation. Future experiments testing these concepts will be required to reach a definitive correlation between water flow in the polymer electrode membrane, the rotational force, and the observed increase in power in the fuel cells.

REFERENCES

[1] V. Fthenakis and H. C. Kim, "Land use and electricity generation: A life-cycle analysis," *Renew. Sustain. Energy Rev.*, vol. 13, no. 6–7, pp. 1465–1474, 2009.

[2] J. Larminie and A. Dicks, *Fuel cell systems explained*, Second Edi. John Wiley & Sons Ltd, The Atrium, Southern Gate, Chichester, West Sussex PO19 8SQ, England, 2003.

[3] F. Barbir, *PEM Fuel Cells : Theory and Practice*. Amsterdam Boston Heidelberg London New York Oxford Paris San Diego San Francisco Singapore Sydney Tokyo: Elsevier Academic Press 30 Corporate Drive, Suite 400, Burlington, MA 01803, USA 525 B Street, Suite 1900, San Diego, California 92101-4495, USA 84 Theobald's Road, London WC1X 8RR, UK, 2005.

[4] I. EG&G Technical Services, *Fuel Cell Handbook*, vol. 7 Edition, no. November. U.S. Department of Energy Office of Fossil Energy National Energy Technology Laboratory P.O. Box 880 Morgantown, West Virginia 26507-0880, 2004.

[5] P. Loyselle and K. Prokopius, "Teledyne Energy Systems , Inc ., Proton Exchange Member (PEM) Fuel Cell Engineering Model Powerplant Test Report : Initial Benchmark Tests in the Original Orientation," no. August, 2011.

[6] Ulf Bossel, "European Fuel Cell Forum. 2002, Literature Review of The Birth of the Fuel Cell (2000)."

[7] Tarek R. Farhat, "A New Concept In Dynamic Hydrogen Fuel Cell: The 'Rotary Fuel Cell.'" Patent Pending, 2006.

[8] T. Van Nguyen and M. Knobbe, "A liquid water management strategy for PEM fuel cell stacks," *J. Power Sources*, 2003.

[9] T. V. Nguyen, "A Water and Heat Management Model for Proton-Exchange-Membrane Fuel Cells," *J. Electrochem. Soc.*, vol. 140, no. 8, p. 2178, 1993.

[10] K. Jiao, B. Zhou, and P. Quan, "Liquid water transport in parallel serpentine channels with manifolds on cathode side of a PEM fuel cell stack," *J. Power Sources*, vol. 154, no. 1, pp. 124–137, 2006.

[11] Y. Wang, K. S. Chen, J. Mishler, S. C. Cho, and X. C. Adroher, "A review of polymer electrolyte membrane fuel cells: Technology, applications, and needs on fundamental research," *Appl. Energy*, vol. 88, no. 4, pp. 981–1007, 2011.

[12] L. B. WANG, N. I. WAKAYAMA, and T. OKADA, "Management of Water Transport in the Cathode of Proton Exchange Membrane Fuel Cells Using Permanent Magnet Particles Deposited in the Cathode-side Catalyst Layer," *ISIJ Int.*, vol. 45, no. 7, pp. 1005–1013, 2005.

[13] X.-G. L. and I.-M. H. Shan-Hai Ge, "Water Management in PEMFCs Using Absorbent Wicks," *J. Electrochem. Soc.*, vol. 151, no. 9, pp. 8523–8528, 2004.

[14] S. A. Mendoza, "Rotary Fuel Cell," *50th AIAA Aerosp. Sci. Meet. Incl. New Horizons*

Forum Aerosp. Expo. 2012 Nashville, Tennessee, USA, 9 - 12 January 2012 Vol. 14 [...], vol. 14, 2012.

[15] "Proton exchange membrane fuel cell," *12 October 2016*. [Online]. Available: https://en.wikipedia.org/wiki/Proton_exchange_membrane_fuel_cell.

[16] C. and S. S. Rayment, *Introduction to Fuel Cell Technology*. 2003.

[17] S. Lindenberg, B. Smith, and K. O'Dell, *20% Wind energy by 2030 Increasing wind Energy's Contribution to U.S. Electricity Supply*. U.S. Department of Energy, 2008.

[18] ENERGY.GOV, "New Interactive Map Shows Big Potential for America's Wind Energy Future." [Online]. Available: https://energy.gov/articles/new-interactive-map-shows-big-potential-america-s-wind-energy-future.

[19] "Wind power provides half of the electricity on US grid for first time ever." [Online]. Available: http://www.independent.co.uk/news/world/americas/wind-power-electricity-half-us-grid-power-record-spp-latest-a7613946.html.

[20] AWEA, "Wind 101: the basics of wind energy." [Online]. Available: http://www.awea.org/wind-energy-101. [Accessed: 03-Sep-2017].

[21] U. of C. Scientists, "How Wind Energy Works." [Online]. Available: http://www.ucsusa.org/clean-energy/renewable-energy/how-wind-energy-works#.WMHWEW_yvcs. [Accessed: 03-Sep-2017].

[22] Electronoic Edition, "Gary L . Johnson," *Wind Energy*.

[23] N. Hoyle and E. Flow, "Royal Academy of Engineering : Renewable Power," *Wind Turbine Power Calc.*, vol. 1, no. 1, pp. 1–5, 2009.

[24] A. W. Manyonge, R. M. Ochieng, F. N. Onyango, and J. M. Shichikha, "Mathematical Modelling of Wind Turbine in a Wind Energy Conversion System: Power Coefficient Analysis," *Appl. Math. Sci.*, vol. 6, no. 91, pp. 4527–4536, 2012.

[25] W. Program, "Wind turbine power ouput variation with steady wind speed." [Online]. Available: http://www.wind-power-program.com/turbine_characteristics.htm.

[26] "Electromagnetic brake," *1/11/2017*. [Online]. Available: https://en.wikipedia.org/wiki/Electromagnetic_brake.

Appendix A. Mean and experiment error of wind turbine shaft torque for varying shaft rpm for different wind tunnel airspeed

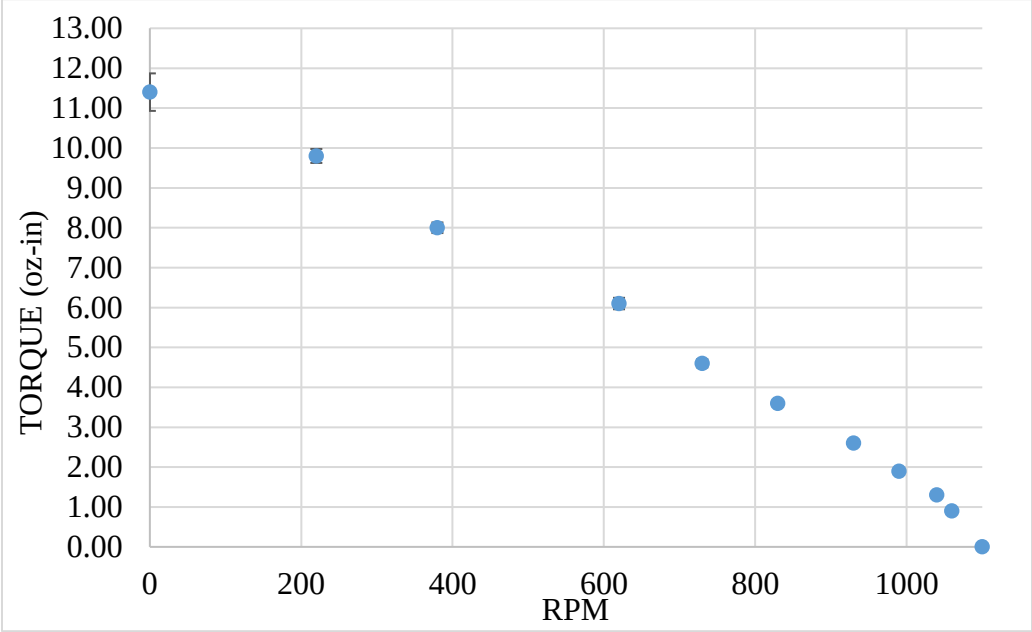

Figure 15. Mean and experiment error of wind turbine shaft torque for varying shaft RPM at 37.2 mph

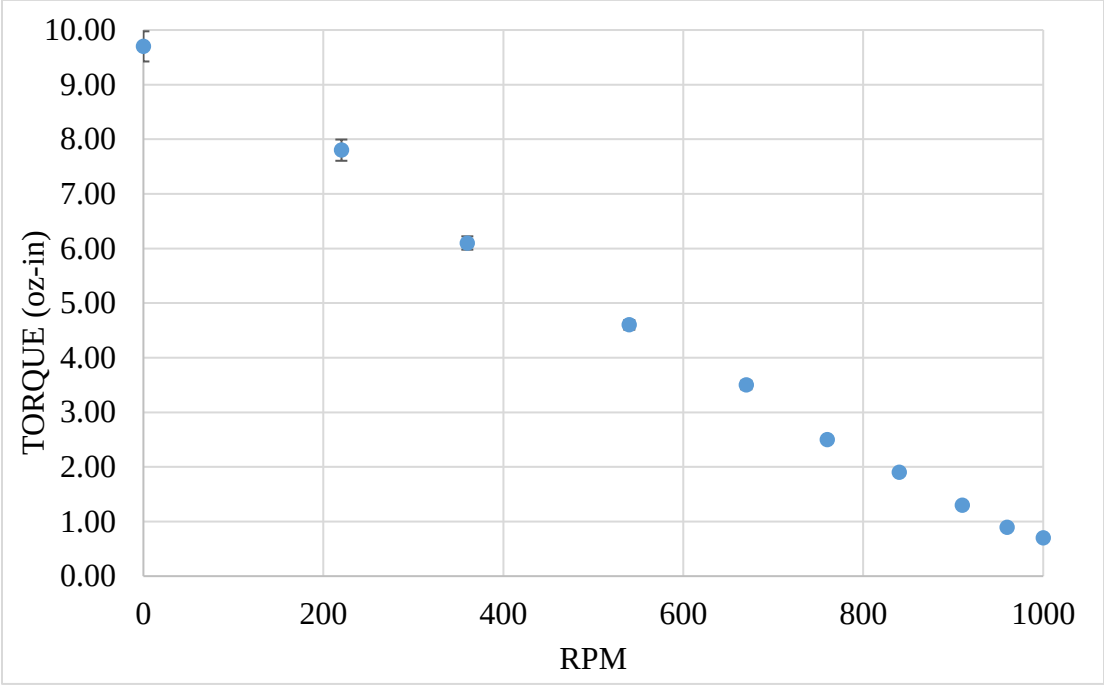

Figure 16. Mean and experiment error of wind turbine shaft torque for varying shaft RPM at 35.7 mph

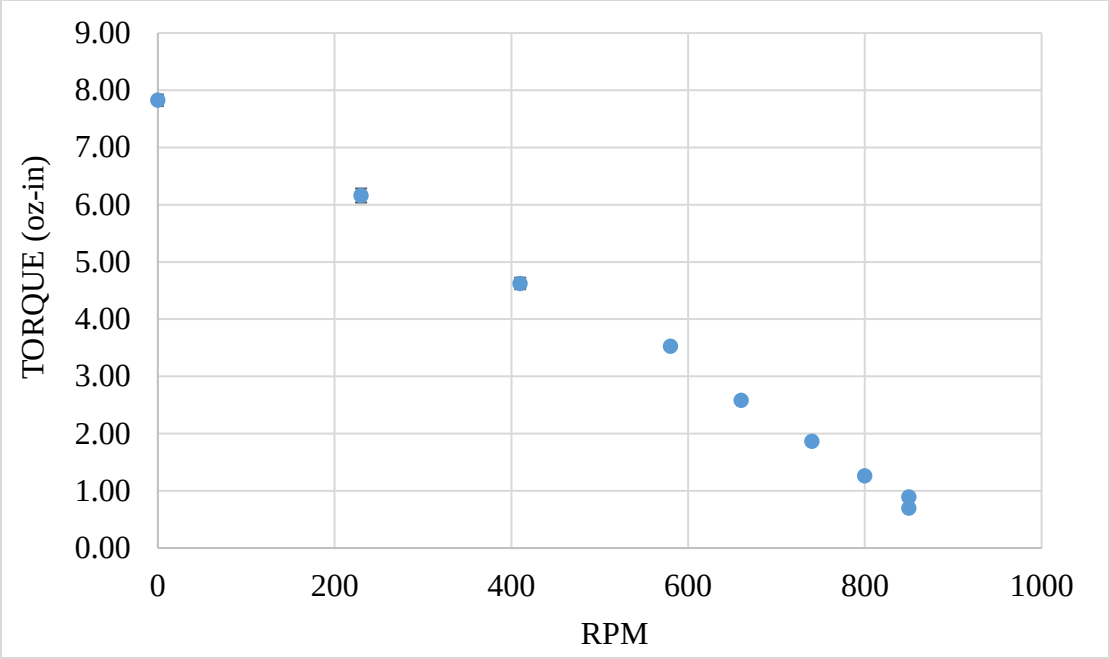

Figure 17. Mean and experiment error of wind turbine shaft torque for varying shaft RPM at 33.6 mph

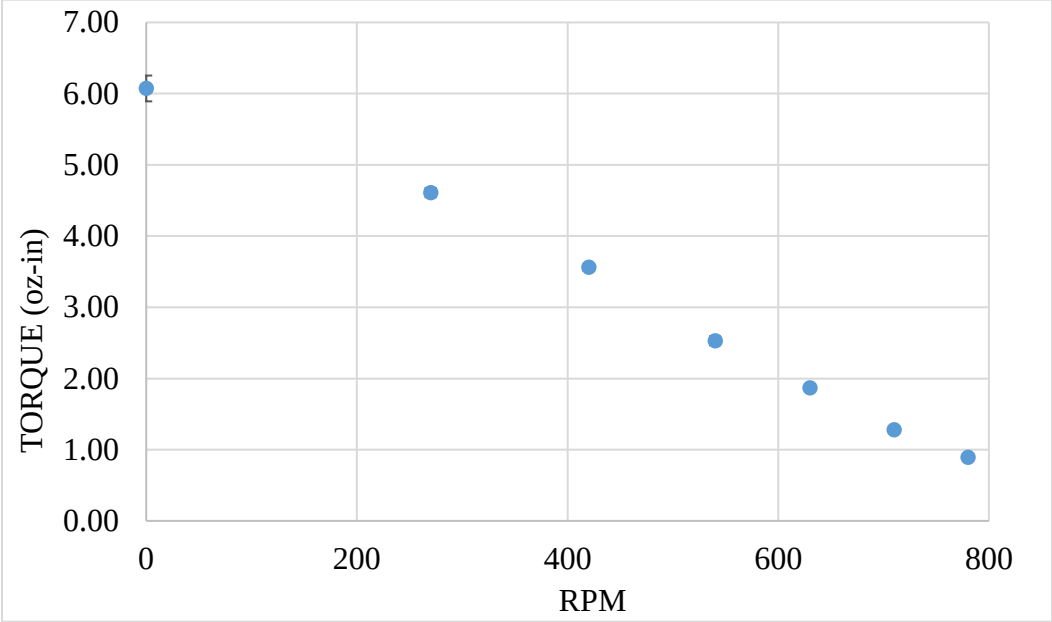

Figure 18. Mean and experiment error of wind turbine shaft torque for varying shaft RPM at 32 mph

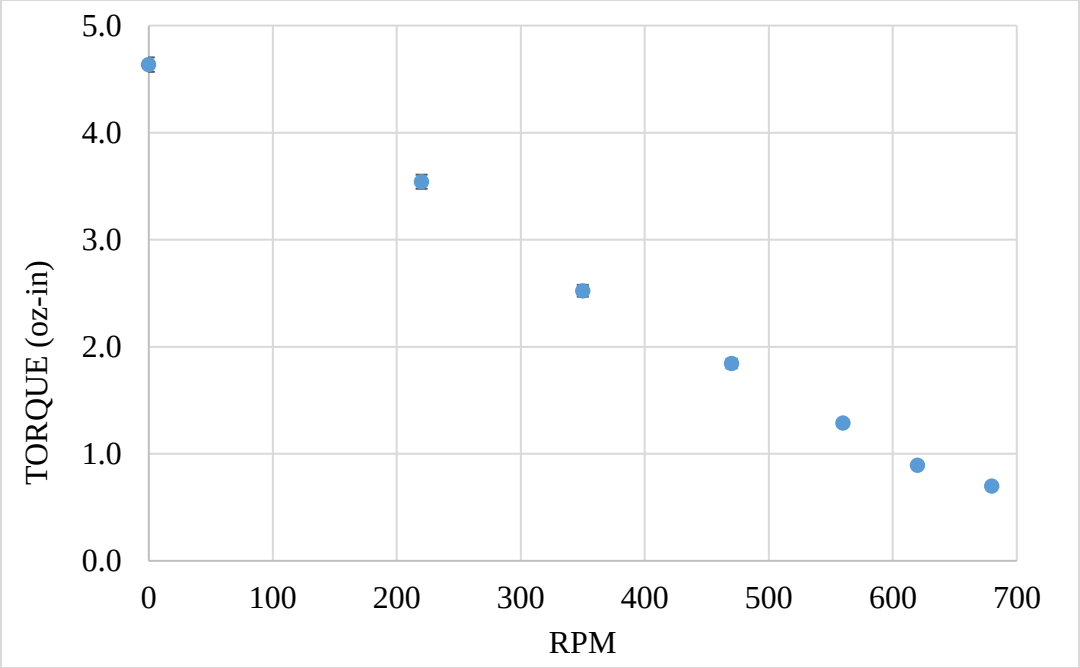

Figure 19. Mean and experiment error of wind turbine shaft torque for varying shaft RPM at 30 mph

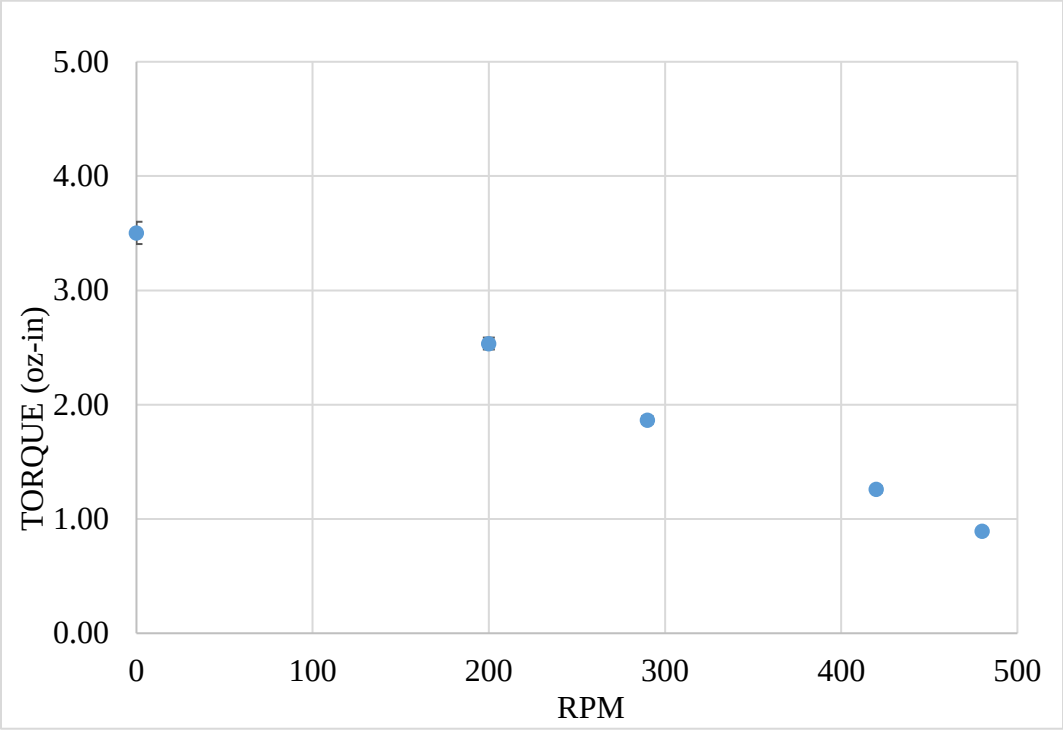

Figure 20. Mean and experiment error of wind turbine shaft torque for varying shaft RPM at 27.4 mph

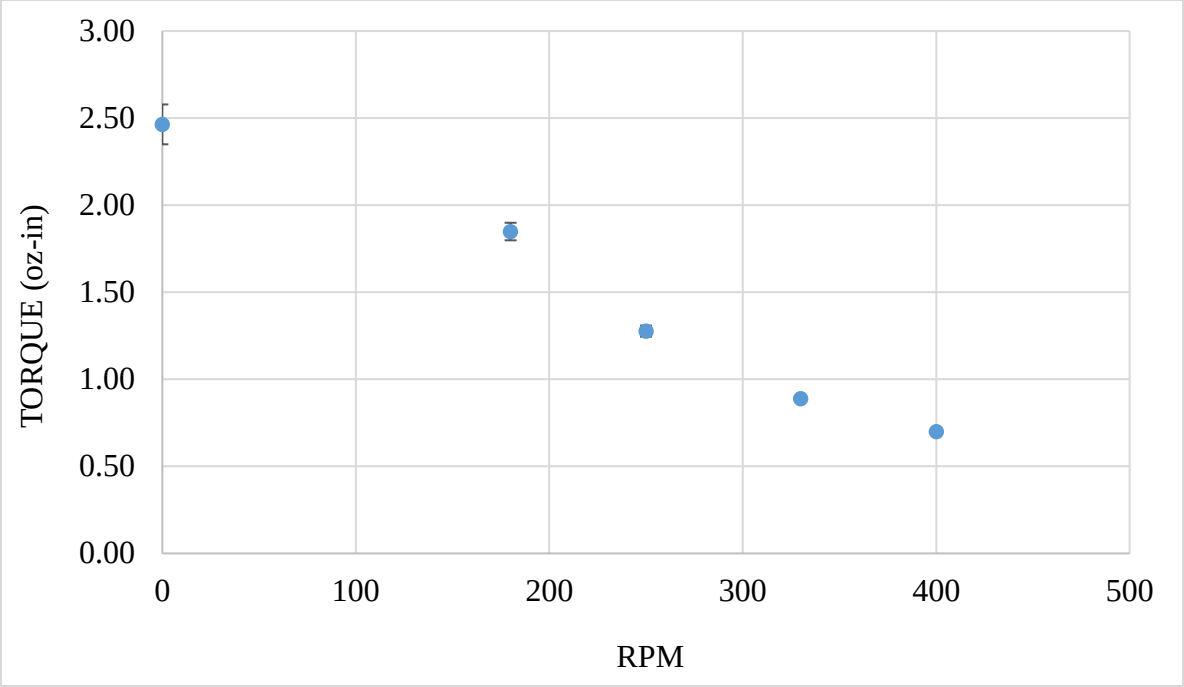

Figure 21. Mean and experiment error of wind turbine shaft torque for varying shaft RPM at 25.3 mph

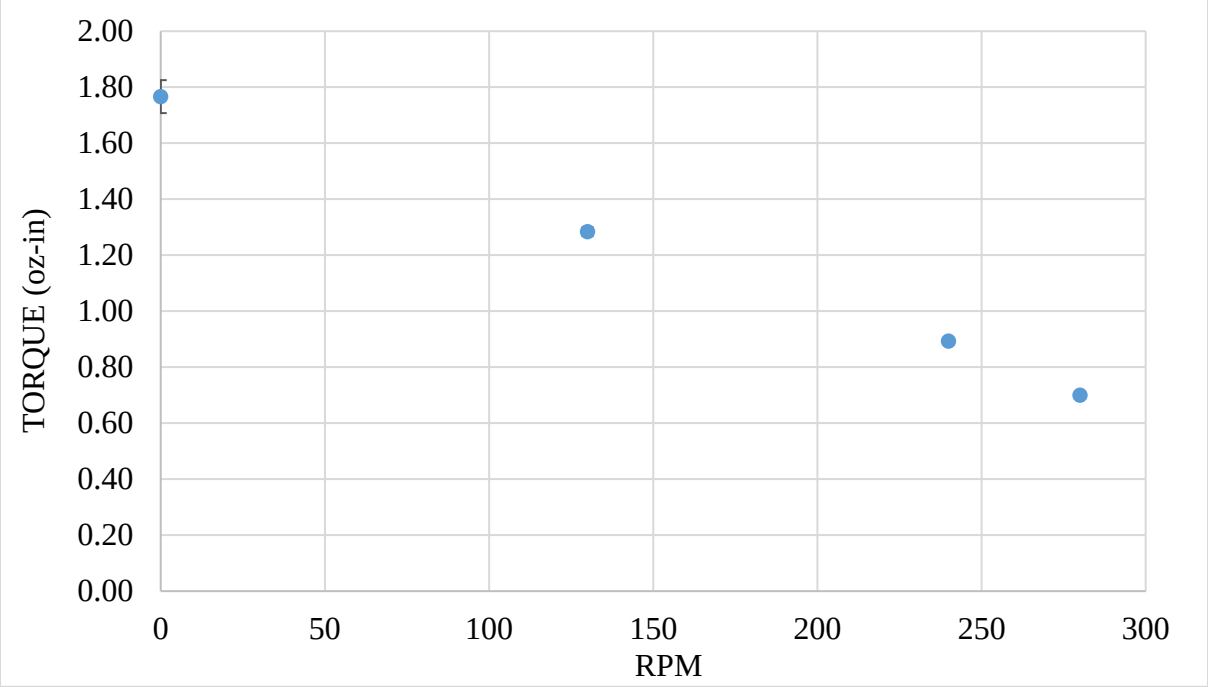

Figure 22. Mean and experiment error of wind turbine shaft torque for varying shaft RPM at 23 mph

Appendix B. Mean and experiment error of wind turbine power output for varying shaft rpm at different wind tunnel airspeed

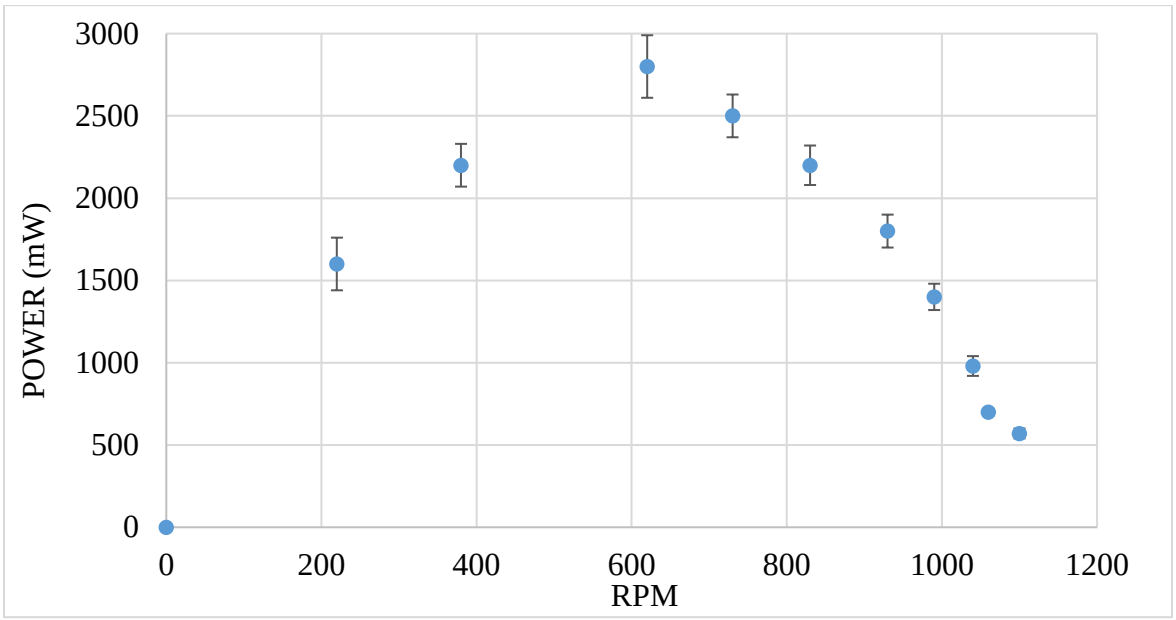

Figure 23. Mean and experiment error of wind turbine power output for varying shaft RPM at 37.2 mph

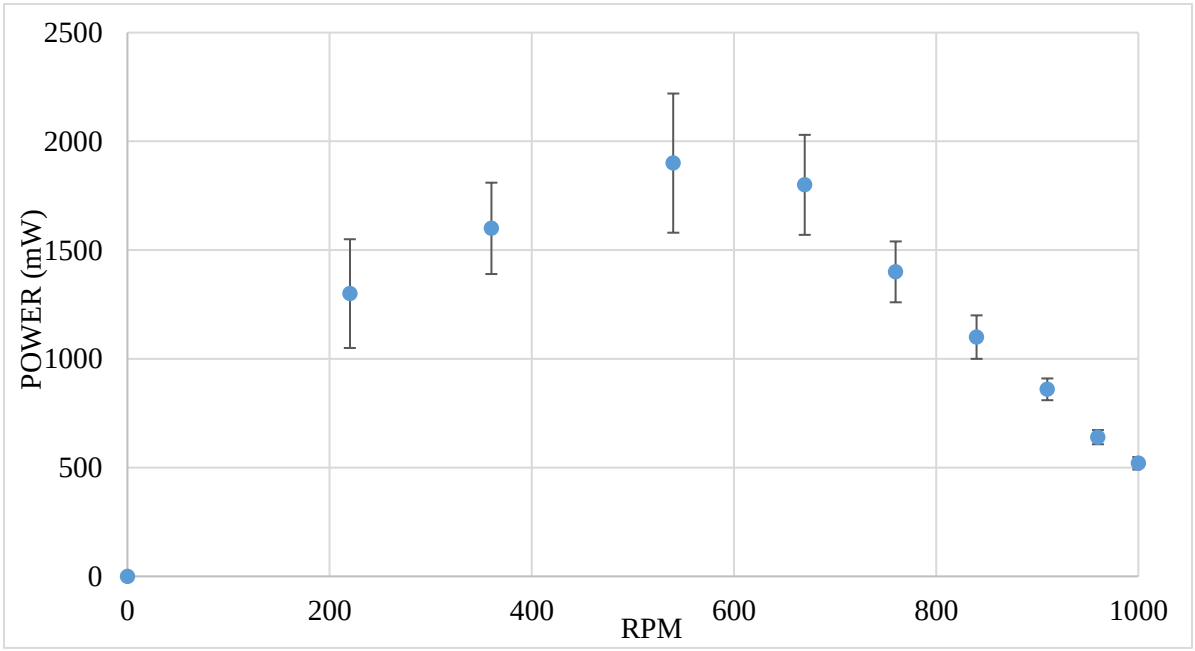

Figure 24. Mean and experiment error of wind turbine power output for varying shaft RPM at 35.7 mph

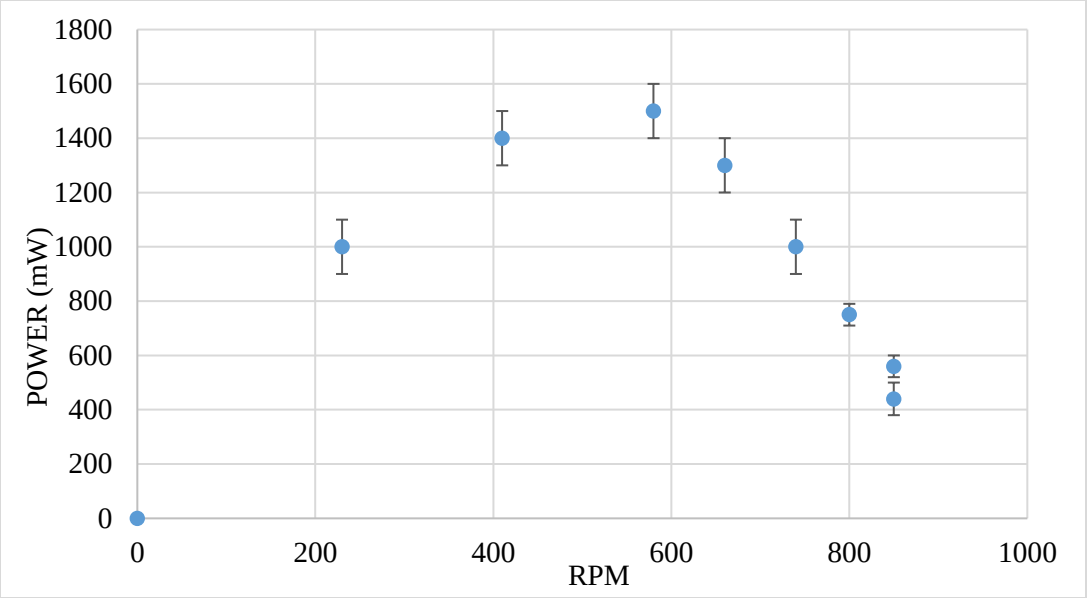

Figure 25. Mean and experiment error of wind turbine power output for varying shaft RPM at 33.6 mph

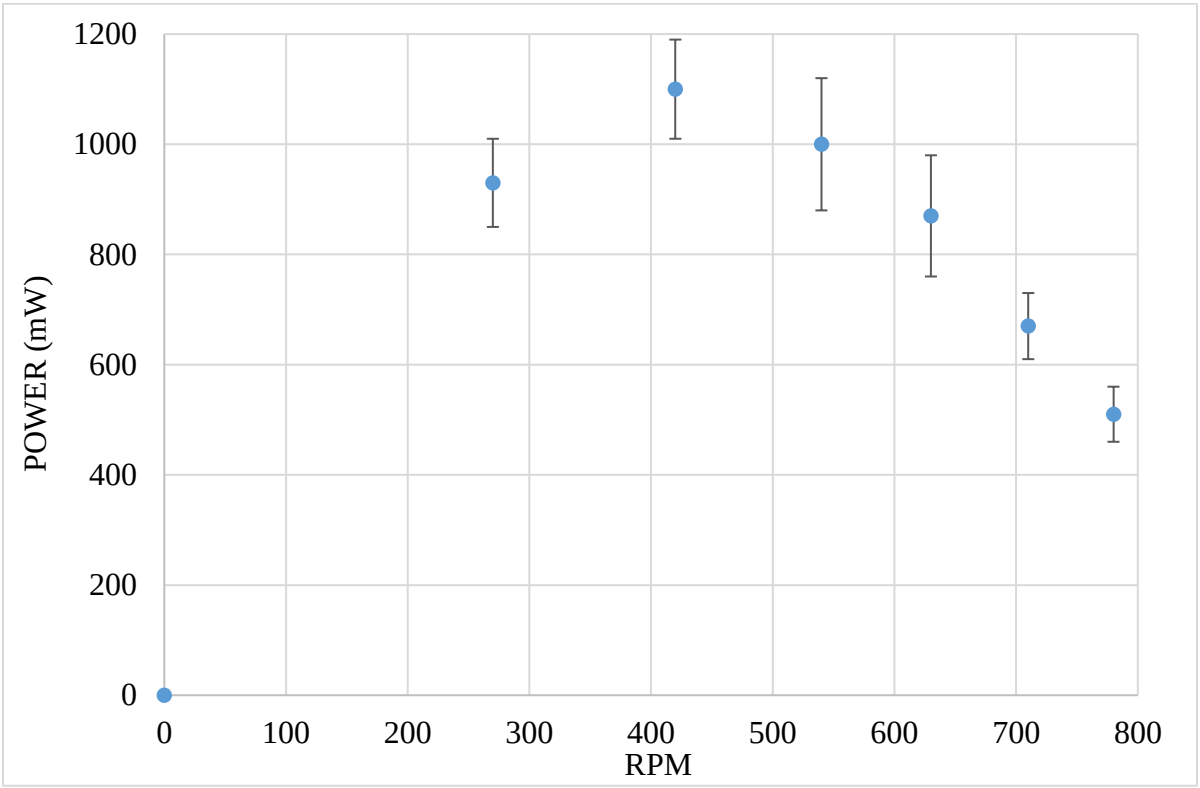

Figure 26. Mean and experiment error of wind turbine power output for varying shaft RPM at 32 mph

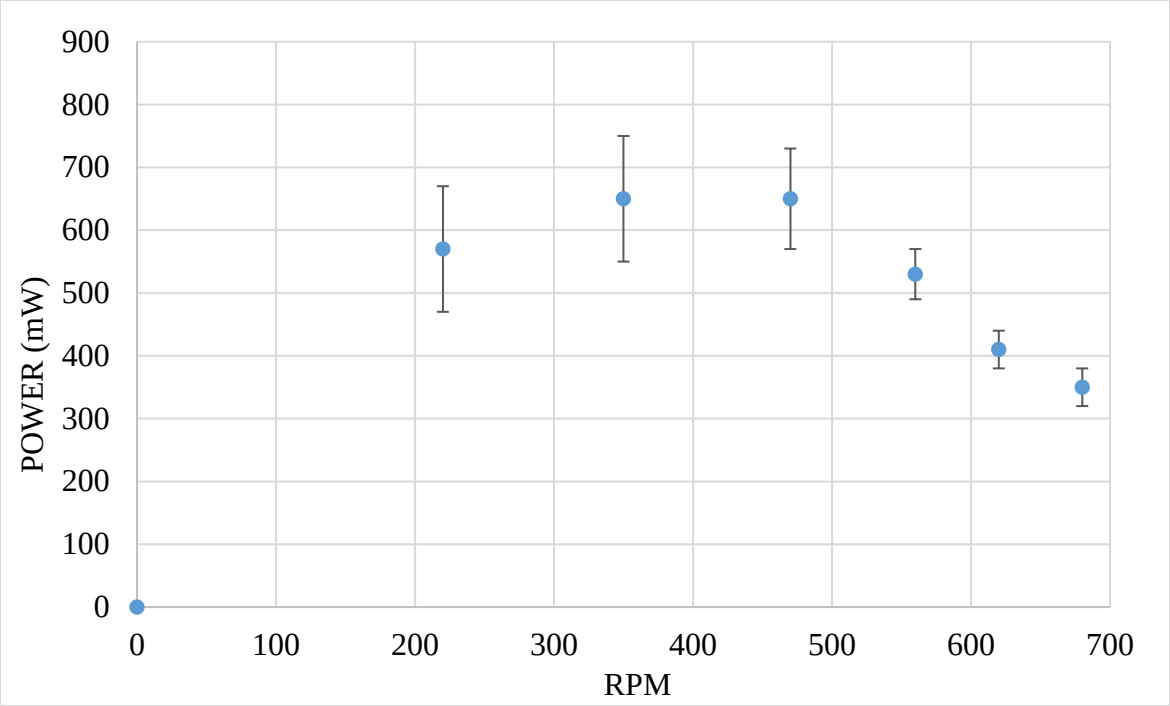

Figure 27. Mean and experiment error of wind turbine power output for varying shaft RPM at 30 mph

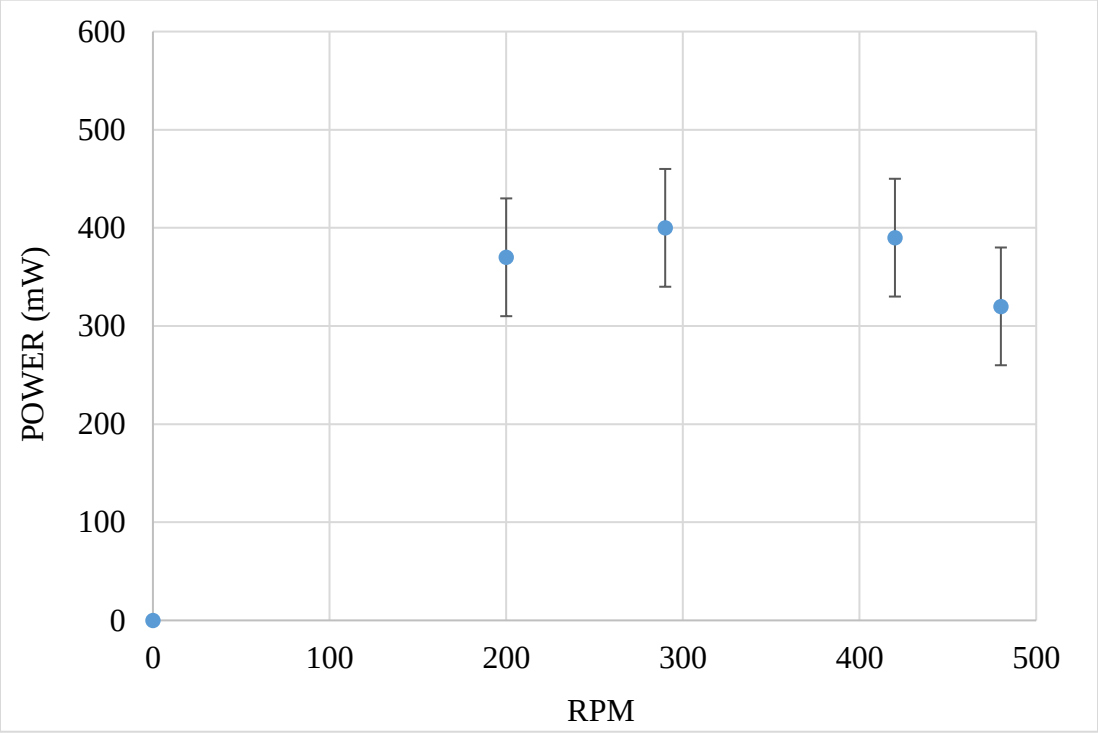

Figure 28. Mean and experiment error of wind turbine power output for varying shaft RPM at 27.4 mph

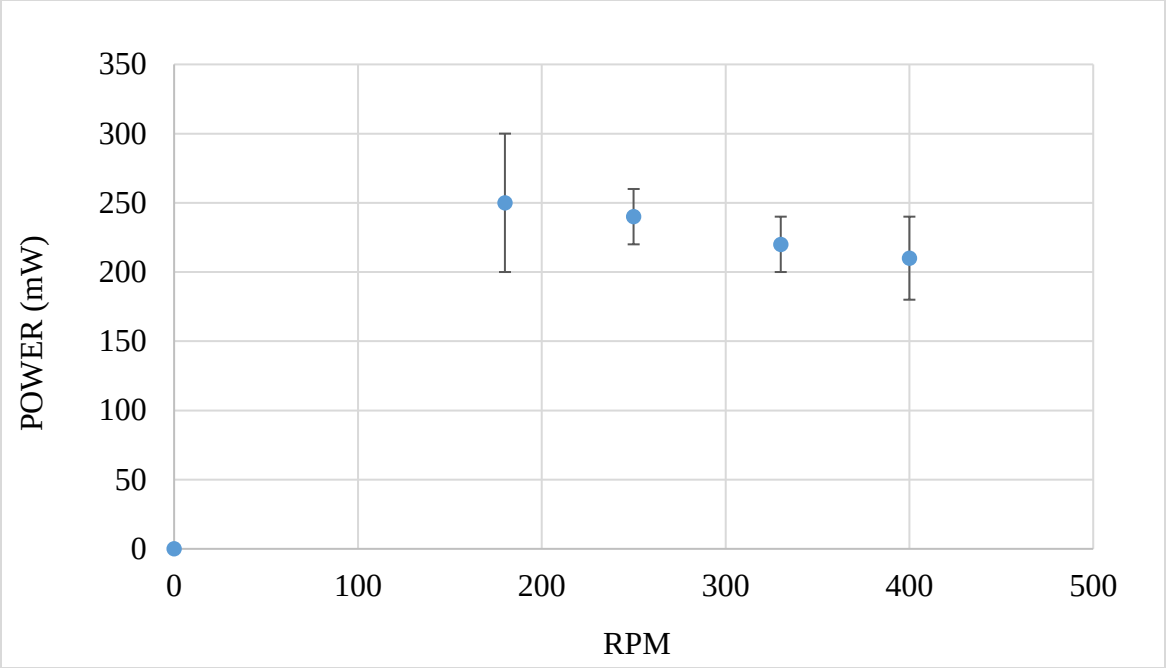

Figure 29. Mean and experiment error of wind turbine power output for varying shaft RPM at 25.3 mph

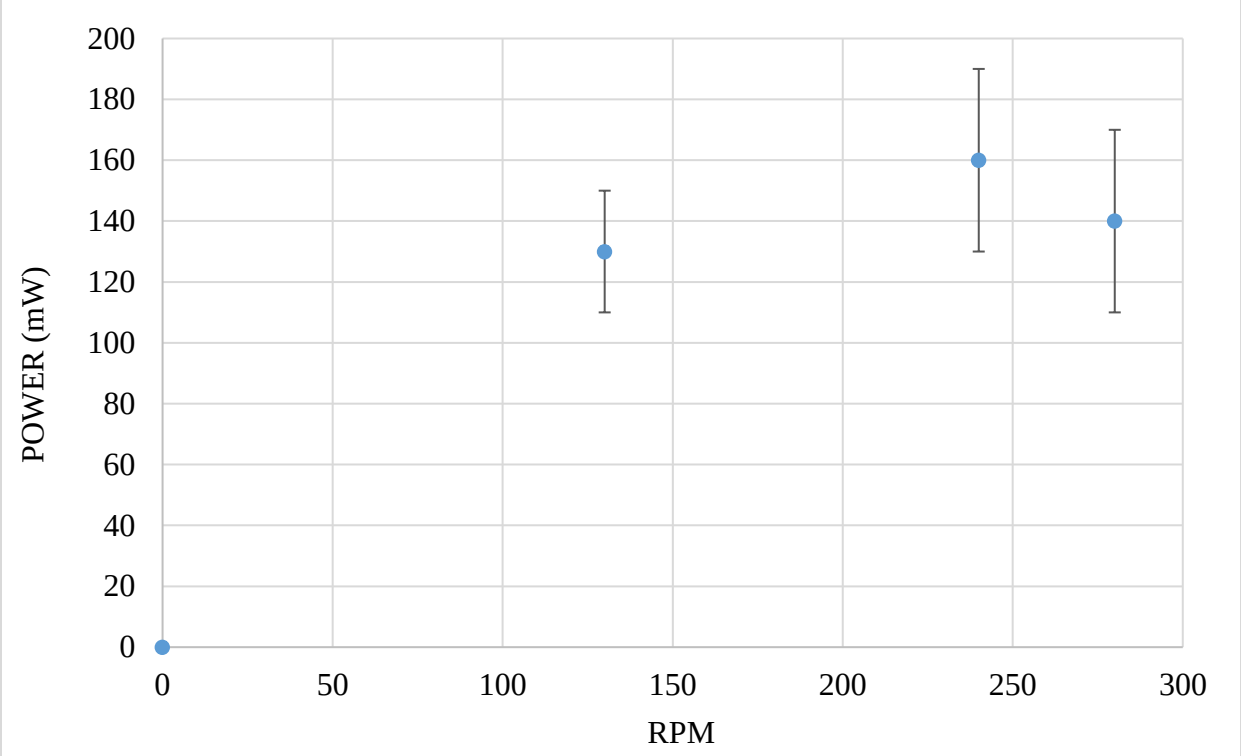

Figure 30. Mean and experiment error of wind turbine power output for varying shaft RPM at 23 mph

Appendix C. Mean and experiment error of fuel cell power output for varying rpm of wind turbine shaft at different wind tunnel airspeed

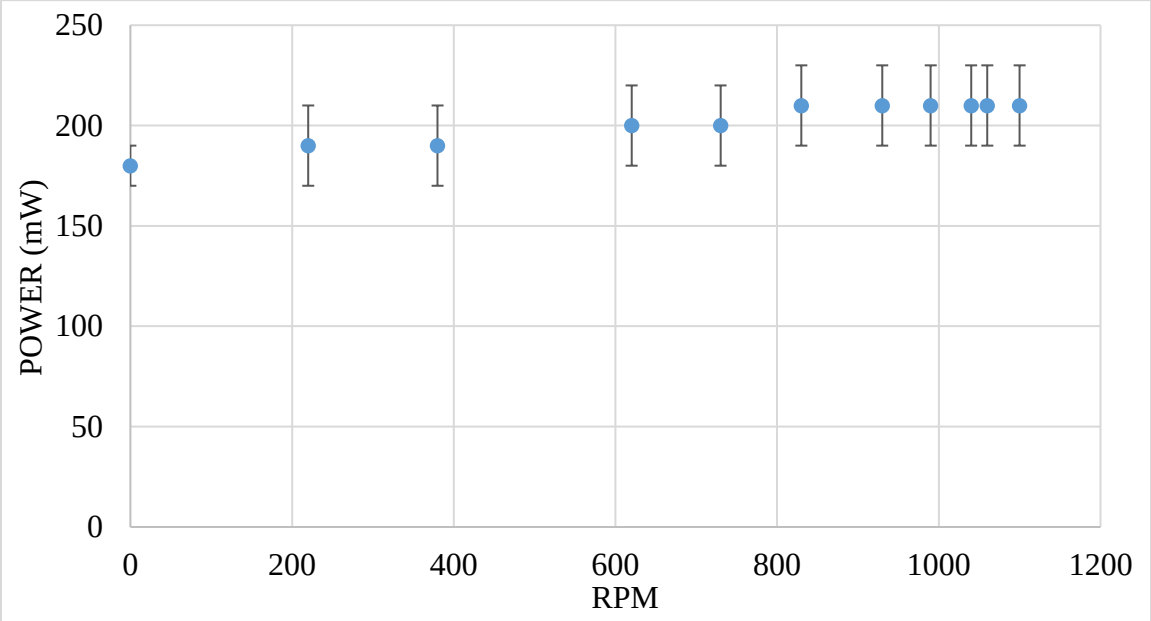

Figure 31. Mean and experiment error of fuel cell power output for varying RPM of the wind turbine shaft at 37.2 mph

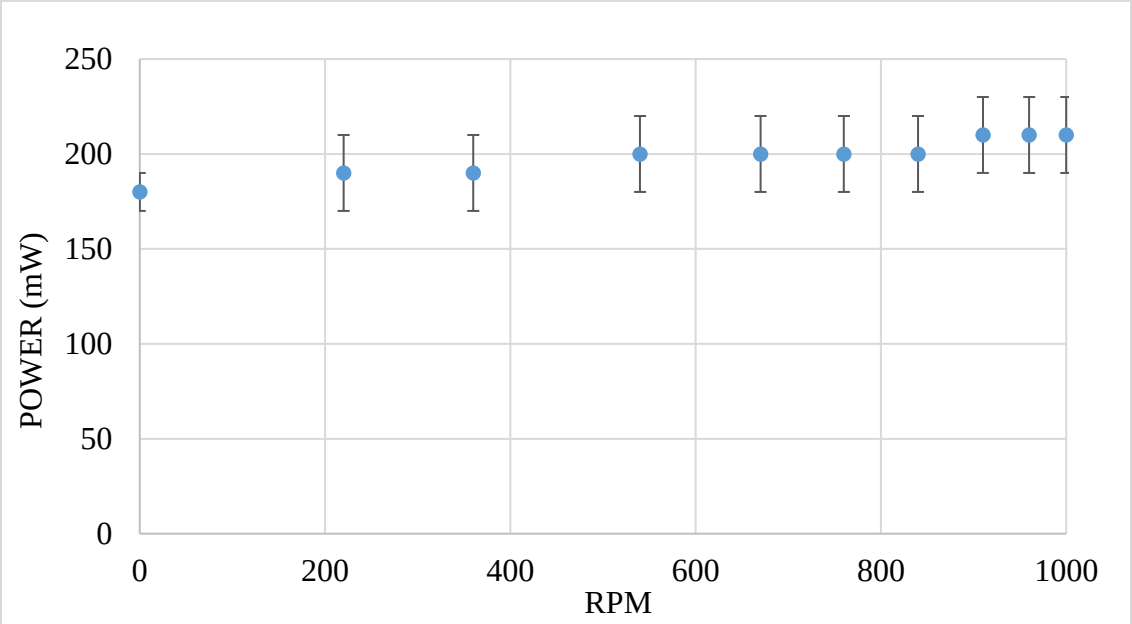

Figure 32. Mean and experiment error of fuel cell power output for varying RPM of the wind turbine shaft at 35.7 mph

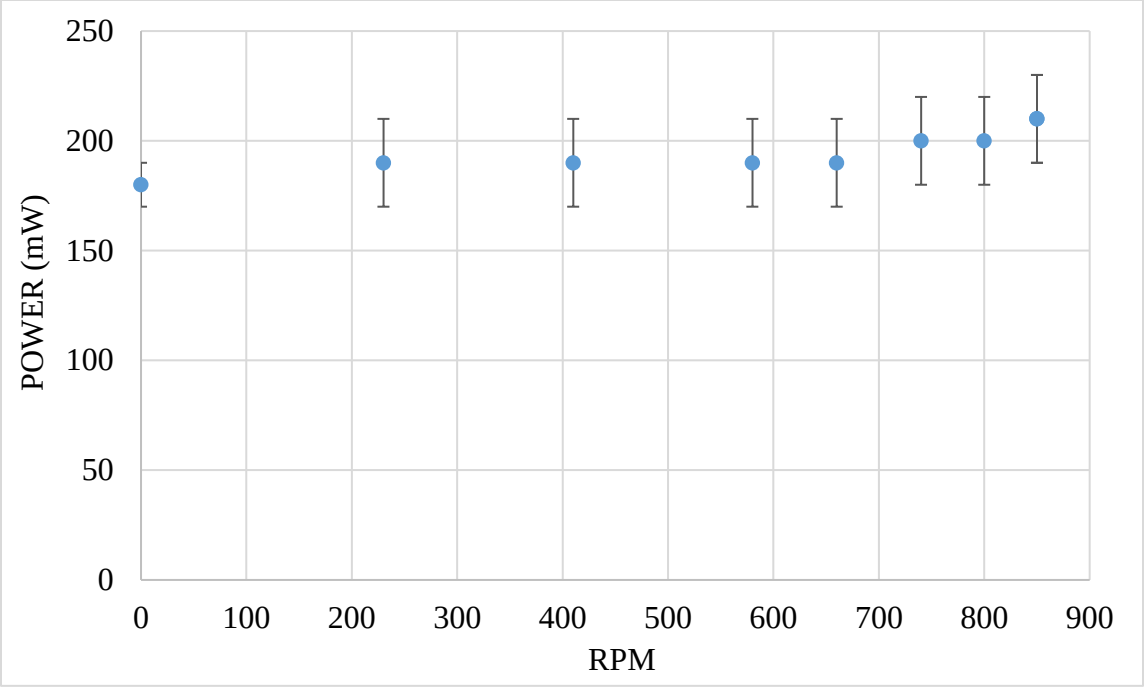

Figure 33. Mean and experiment error of fuel cell power output for varying RPM of the wind turbine shaft at 33.6 mph

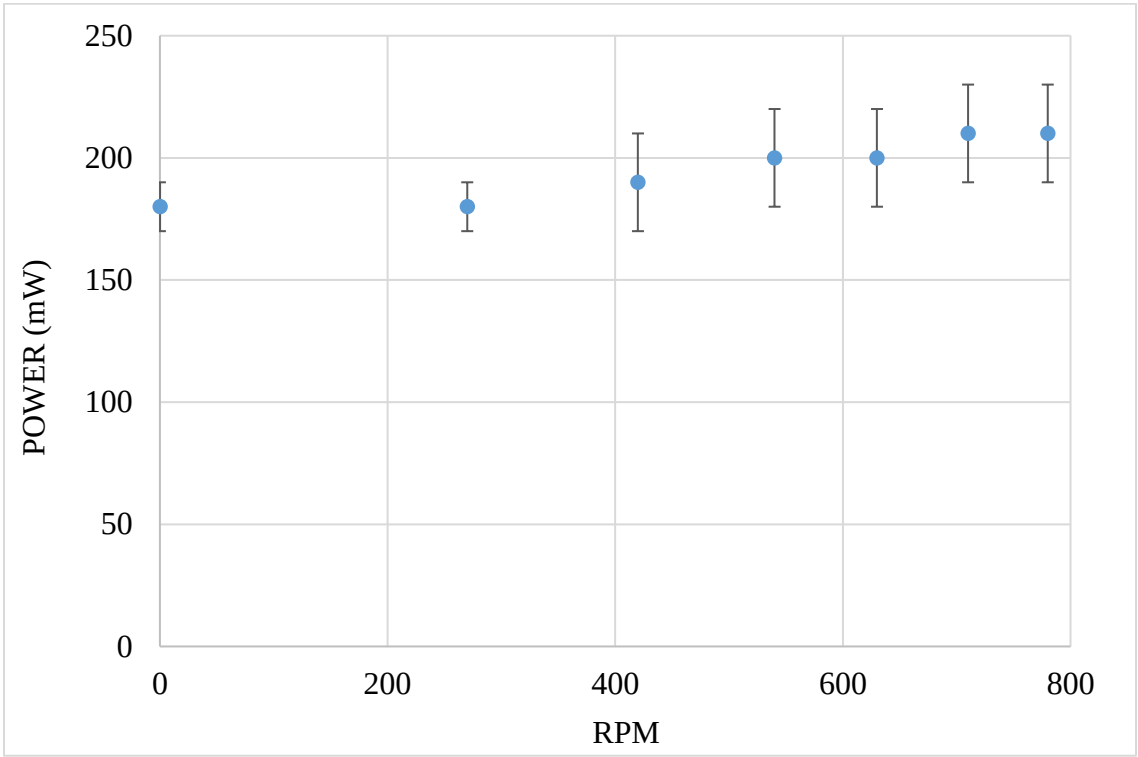

Figure 34. Mean and experiment error of fuel cell power output for varying RPM of the wind turbine shaft at 32 mph

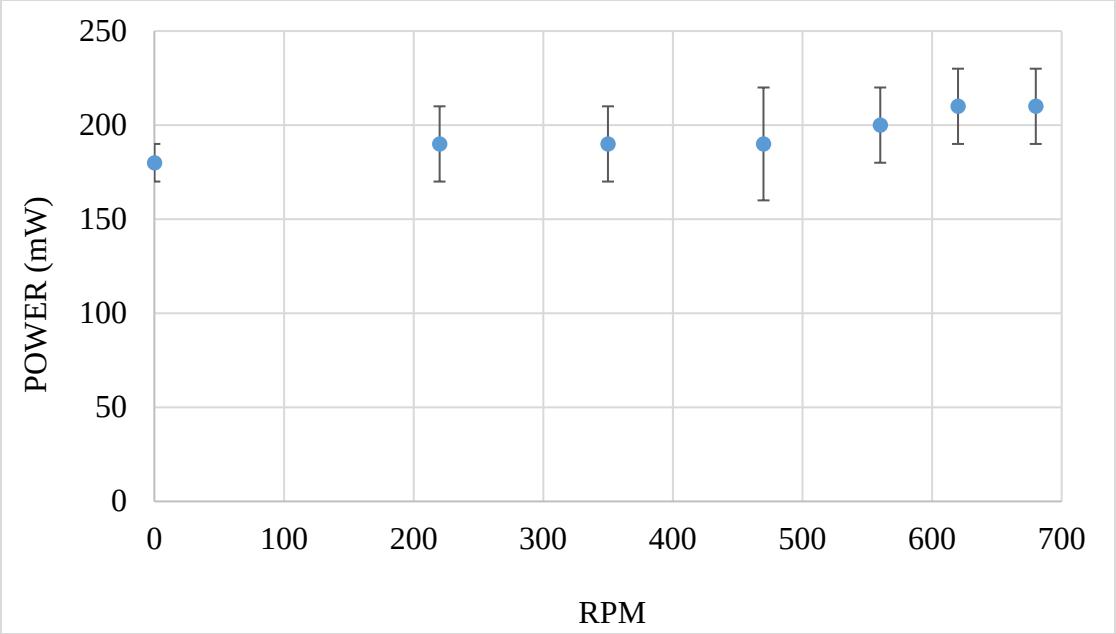

Figure 35. Mean and experiment error of fuel cell power output for varying RPM of the wind turbine shaft at 30 mph

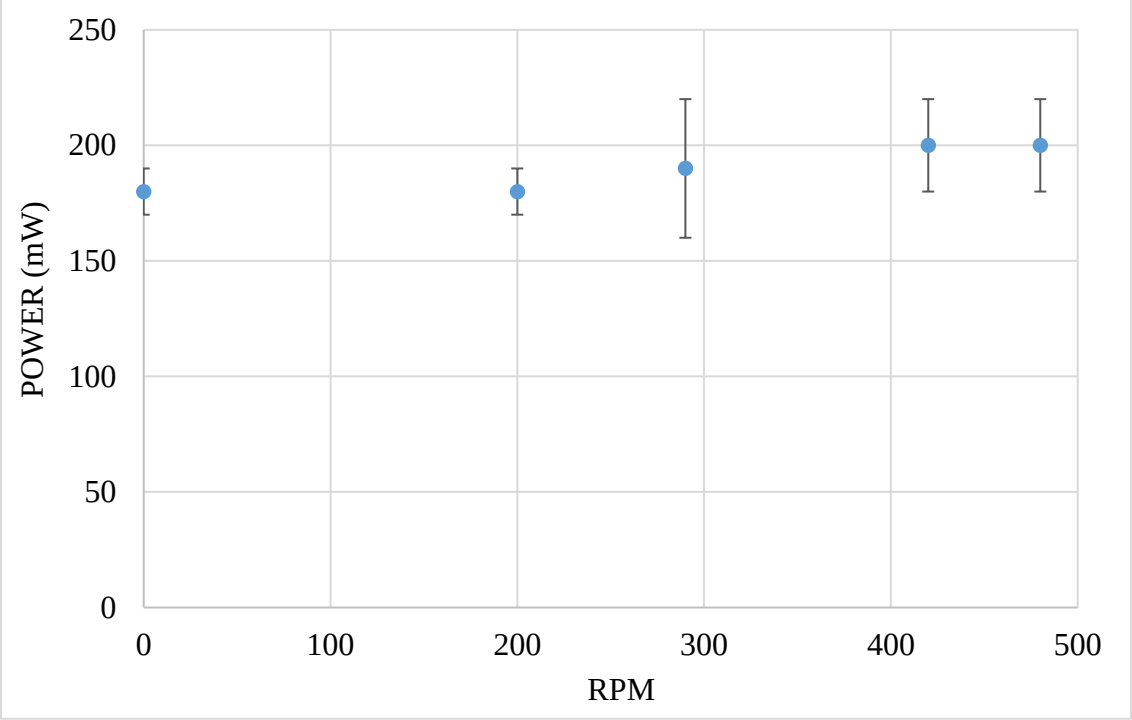

Figure 36. Mean and experiment error of fuel cell power output for varying RPM of the wind turbine shaft at 27.4 mph

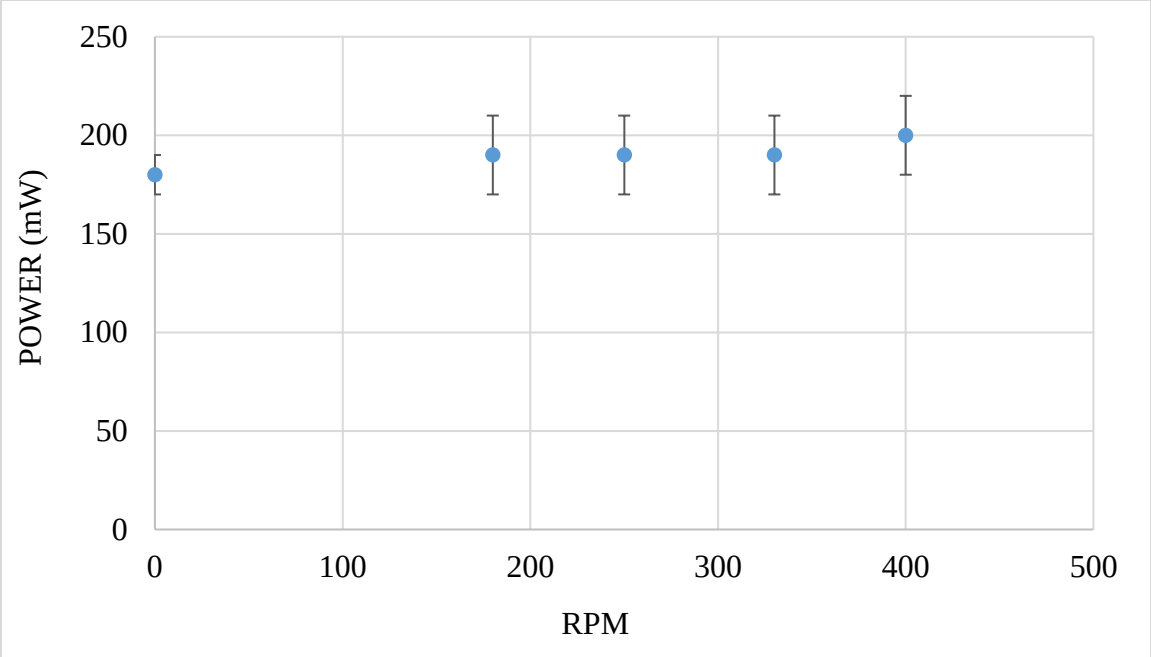

Figure 37. Mean and experiment error of fuel cell power output for varying RPM of the wind turbine shaft at 25.3 mph

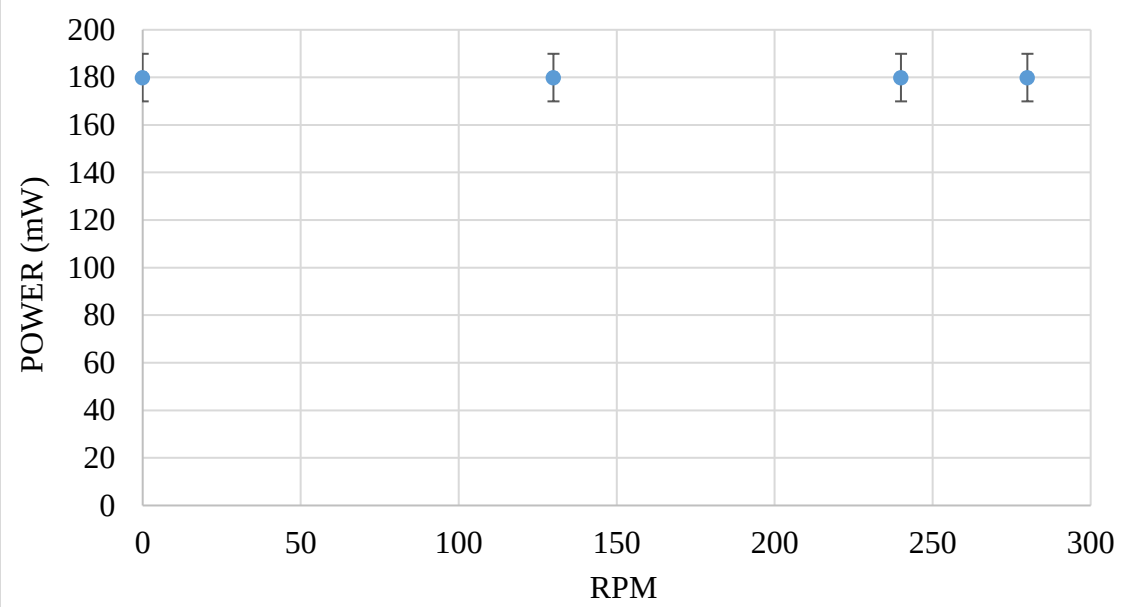

Figure 38. Mean and experiment error of fuel cell power output for varying RPM of the wind turbine shaft at 23 mph